

Rotation and spots in normal A and Am/Fm stars

Otto Trust¹[★], Edward Jurua¹[†], Peter De Cat² and Santosh Joshi³

¹*Department of Physics, Mbarara University of Science and Technology, P.O. Box 1410, Mbarara, Uganda*

²*Royal Observatory of Belgium, Ringlaan 3, B-1180 Brussel, Belgium*

³*Aryabhatta Research Institute of Observational Sciences, Manora Peak, Nainital- 263002, India*

Accepted XXX. Received YYY; in original form ZZZ

ABSTRACT

Frequency analysis of long-term ultra-precise photometry can lead to precise values of rotation frequencies of rotating stars with “hump and spike” features in their periodograms. Using these features, we computed the rotation frequencies and amplitudes. The corresponding equatorial rotational velocity (V_{rot}) and spot size were estimated. On fitting the autocorrelation functions of the light-curves with the appropriate model, we determined the starspot decay-time scale. The V_{rot} agrees well with the projected rotational velocity ($v \sin i$) in the literature. Considering a single circular and black spot we estimate its radius from the amplitude of the “spike”. No evidence for a significant difference in the average “spike” amplitude and spot radius was found for Am/Fm and normal A stars. Indeed, we derived an average value of $\sim 21 \pm 2$ and $\sim 19 \pm 2$ ppm for the photometric amplitude and of 1.01 ± 0.13 and $1.16 \pm 0.12 R_E$ for the spot radius (where R_E is the Earth radius), respectively. We do find a significant difference for the average spot decay-time scale, which amounts to 3.6 ± 0.2 and 1.5 ± 0.2 days for Am/Fm and normal A stars, respectively. In general, spots on normal A stars are similar in size to those on Am/Fm stars, and both are weaker than previously estimated. The existence of the “spikes” in the frequency spectra may not be strongly dependent on the appearance of starspots on the stellar surface. In comparison with G, K and M stars, spots in normal A and Am/Fm stars are weak which may indicate the presence of a weak magnetic field.

Key words: stars: chemically peculiar – stars: rotation – stars: starspots – stars: general

1 INTRODUCTION

The main sequence A-type stars are intermediate-mass stars which show various interesting phenomena such as chemical peculiarities, pulsation, activity and rotation. The chemically peculiar (CP) stars (Preston 1974; Renson 1988; Monier 2019) can be distinguished from the normal A stars (Adelman 1986, 2004) based on the enhancement of the absorption lines in their spectra. The optical spectra of the CP stars are characterized by strong lines of silicon, metals and/or rare-earth elements and weak lines of calcium. The CP stars are dominated by metallic line (Am/Fm) stars and are sub-divided into two main groups: the Am/Fm stars, (CP1; having an over-abundance of iron-group metals and an under-abundance of He, Ca and/or Sc in their atmospheres), and the magnetic Ap stars (CP2; showing photometric and magnetic variability and having abnormally strong lines of

Si, Cr, Sr and rare-earth elements in their spectra) (Conti 1970; Preston 1974; Fossati et al. 2009).

The atomic diffusion is thought to be the dominant process responsible for the chemical anomalies observed in the CP stars (Michaud 1970; Watson 1970; Khokhlova 1981; Hui-Bon-Hoa 2000; Turcotte 2003; Théado et al. 2011). Due to radiation pressure and gravitational settling, chemical elements undergo an upward/downward drift into/out of the atmosphere. Depending on the ionization state and the atomic properties of the elements and in the absence of mixing, an equilibrium is attained. At equilibrium, the elements are vertically stratified (Ryabchikova et al. 2002; Khalack & LeBlanc 2015) and the abnormal chemical abundances manifest in the atmospheres. In Am/Fm stars, when the magnetic fields are detected, they are ultra-weak and relatively uniform (e.g; Aurière et al. 2010; Blazère et al. 2014; Blazère et al. 2016a; Neiner et al. 2017; Cantiello & Braithwaite 2019) which produce evenly distributed abundances in the atmospheres. On the other hand, Ap stars possess strong global magnetic fields of the range 200 G–30 kG (Power et al.

* E-mail: otrust@must.ac.ug

† E-mail: ejurua@must.ac.ug

2007; Braithwaite 2014). In these stars, depending on the magnetic field strength which may suppress convection and the inclination of the field lines, patches of different abundances are produced on the surface (Michaud 1970; Mullan 1973).

The atomic diffusion can be counteracted by mixing. The currently known mixing processes include meridional circulation caused by rotation, and convection. This implies that the CP stars should be rotating more slowly relative to normal A stars. The majority of Am/Fm stars are indeed slow rotators (Takeda et al. 2008; Fossati et al. 2008; Stateva et al. 2009), with $v \sin i < 120 \text{ km s}^{-1}$ (Abt 2009). The slow rotation in Am/Fm stars is attributed to the tidal synchronisation in the case of close binaries (Khokhlova 1981; Kunzli & North 1998; Balona et al. 2011). The Am/Fm stars are often components of binaries (Abt 1961; Vauclair 1976; North et al. 1998; Debernardi 2000; Stateva et al. 2009) with orbital periods between 1 and 10 days (Smalley et al. 2014). This makes rotation one of the most important phenomena in stellar physics. The availability of accurate and precise values of rotation periods provides an important platform in understanding other stellar phenomena such as pulsation (Dziembowski et al. 1988; Soufi et al. 1998) and overshooting (Browning et al. 2004; Costa et al. 2019) and allows to draw conclusions about the processes that may be linked with the observed chemical abundances in stellar atmospheres of Am/Fm stars (Turcotte 2001; Murphy 2014). The other reported success of the rotationally induced mixing is the ability to explain the origin of the Boesgaard lithium gap (Boesgaard & Tripicco 1986) in F stars (Sills & Deliyannis 2000). Apart from using spectroscopy, where the rotation rate is retrieved from the broadening of the absorption lines (Kaler 1989), stellar rotation period can be determined from seismic splitting (Saio 1981; Claverie et al. 1981), spot induced rotational modulation (Kron 1947; Mosser et al. 2009) and chromospheric activity especially Ca II emission (Noyes et al. 1984).

Thanks to the availability of high-precision and almost continuous photometric data from space missions like the nominal *Kepler* mission (Borucki et al. 2010), K2 (Howell et al. 2014) and the Transiting Exoplanet Survey Satellite (*TESS*; Ricker et al. 2014), from which precise rotation periods can be obtained. Balona (2013) derived rotation periods of a large number of A-type stars from the original *Kepler* field (Borucki et al. 2010) based on spot induced rotational modulation. Starspots and flares are claimed to have been discovered in rotationally modulated normal A and Am/Fm stars (Balona 2012, 2013; Balona et al. 2015; Balona et al. 2016). Balona (2013) obtained a mean rotational modulation amplitude, interpreted as a reflection of the starspot size, of 875 normal A stars as $541 \pm 86 \text{ ppm}$ and Balona et al. (2015) found $93 \pm 25 \text{ ppm}$ for 10 Am/Fm stars. As starspots and flares are signatures of a high magnetic field, this would imply a strong magnetic field in these stars. Pedersen et al. (2017) confirmed the presence of flare-like structures in only some stars studied by Balona (2012, 2013). However, after consideration of different possibilities, Pedersen et al. (2017) found that the flare-like structures have a high possibility of originating from cool and unresolved companions.

The discovery of spot based rotational modulation in normal A and Am/Fm stars was unexpected. They possess a thin sub-surface convective envelope, which increases in

depth with decreasing effective temperature and decreasing surface gravity (Giampapa & Rosner 1984; Abt 2009). This implies that they lack strong tangled magnetic fields which would be created by the dynamo effect resulting from the convective behavior of the material with rotation (Brandenburg 2000) like in G, K and M stars. Aurière et al. (2007) reported that stellar magnetic fields of magnitude below 300 G are not detected. However, ultra-weak global magnetic fields have been observed in a number of stars, e.g; normal A-type stars, like Vega ($0.6 \pm 0.3 \text{ G}$; Lignières et al. 2009), (1.0 G and 1.4 G ; Petit et al. 2010), (7.0 G ; Petit et al. 2014) and Am/Fm stars, like Sirius A ($0.2 \pm 0.1 \text{ G}$) (Petit et al. 2011), Alhena (around $5 \pm 3 \text{ G}$) (Blazère et al. 2016a), $\beta \text{ UMa}$ ($1 \pm 0.8 \text{ G}$) and $\theta \text{ Leo}$ ($0.4 \pm 0.3 \text{ G}$) (Blazère et al. 2016b) and $\rho \text{ Pup}$ ($0.29 \pm 0.32 \text{ G}$) (Neiner et al. 2017). Cantiello & Braithwaite (2019) theoretically predicted that A-stars like Vega, Sirius, $\beta \text{ UMa}$, $\theta \text{ Leo}$ and Alhena can have magnetic fields of magnitude of $1 - 10 \text{ G}$ generated by dynamo action in the thin He II convective subsurface zone and transported to the surface by magnetic buoyancy. Magnetic fields with such magnitude and the thin convective zone could support, if any, weak starspots (Blazère et al. 2016a; Neiner et al. 2017; Cantiello & Braithwaite 2019). Therefore, spot sizes in normal A and Am/Fm stars given by Balona (2013) and Balona et al. (2015), respectively, could be overestimated.

In addition, Balona (2013) observed in the frequency spectra of 135 stars of the 875 normal A stars a sharp peak (“spike”) on the high frequency side of a broad hump of very close frequencies (“hump”) as shown in Fig. 1. The sharp frequency and the broad hump were seen to have harmonics of lower amplitudes in most cases. Balona et al. (2015) observed the same scenario in some Am/Fm stars. Balona (2014) suspected the sharp peak corresponds to the rotational frequency and its amplitude to be related to the starspot size, but the hump remained unexplained. Recently, Saio et al. (2018) named these stars “hump and spike” stars. Saio et al. (2018) carefully compared the visibility curves for the global Rossby waves (*r*modes) (Papaloizou & Pringle 1978) with the frequency spectra of *Kepler* light curves and concluded that the broad humps as observed for these stars are induced by *r*modes and the spike structures are the rotation frequencies induced by one or more spots.

To search and study the pulsational variabilities in Ap and Am/Fm stars, a dedicated ground-based project the “Nainital-Cape Survey” was initiated between astronomers of India and South Africa. However, with time, astronomers from other institutions in other countries joined this programme making it a multi-national collaborative project and a number of results are published (e.g; Ashoka et al. 2000; Martinez et al. 2001; Joshi et al. 2003, 2006, 2009, 2010, 2012, 2016, 2017). The success of the “Nainital-Cape Survey” and the discovery of “hump and spike” features in the frequency spectra (Balona 2013; Balona et al. 2015; Saio et al. 2018) of a number of normal A and Am stars motivated us to initiate another tri-national collaborative group among the astronomers from India, Uganda and Belgium. This paper is the first of the series involving the “hump and spike” stars aiming to present rotation frequencies and velocities, starspot sizes and starspot decay life-times based on the “hump and spike” features. Only normal A and Am/Fm stars in the original *Kepler* field with “hump and spike” features in their frequency spectra are investigated. This paper

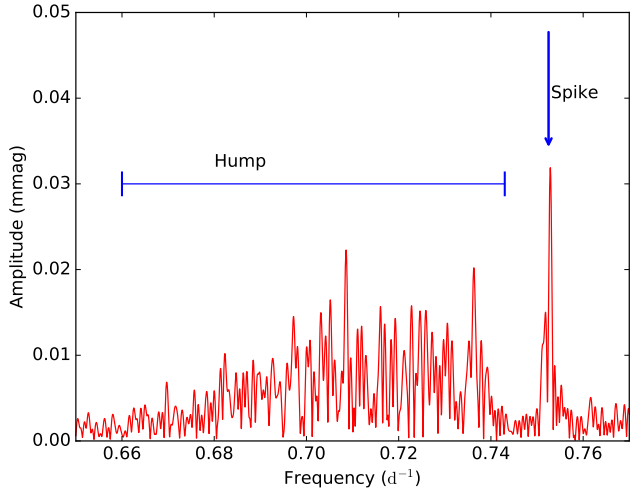


Figure 1. An amplitude spectrum of KIC 6192566 showing a typical hump and a spike. The spike is not strictly sharp.

is organized follows. The adopted target selection criteria and the data reduction are described in Section 2. The results and their discussion are presented in Section 3. The conclusion drawn from our study is given in Section 4.

2 TARGET SELECTION AND DATA REDUCTION

2.1 Selection criteria

The samples in this study were drawn from stars analysed by Balona (2013), Balona et al. (2015), and Gray et al. (2016). Of the 875 rotationally modulated main sequence normal A stars studied by Balona (2013) and the 15 Am/Fm stars from the nominal *Kepler* mission analysed by Balona et al. (2015), only the normal A and Am/Fm stars with “hump and spike” features in their frequency spectra were considered. Additional Am/Fm stars with “hump and spike” features in the frequency spectra were derived from the sources analysed by Gray et al. (2016) under the LAMOST-*Kepler* project (De Cat et al. 2015). A total of 170 “hump and spike” stars were obtained of which 131 are part of the normal A stars reported by Balona (2013), 3 are within the sample studied by Balona et al. (2015), and 36 are from Gray et al. (2016).

2.2 Data reduction

For this study, we used the high precision and almost continuous photometric data obtained by the *Kepler* mission. The data are available on the Barbara A. Mikulski Archive for Space Telescopes (MAST) website¹. The stars in the sample were observed in the long-cadence mode with an observation every 29.4 minutes. A few of the “hump and spike” stars were also observed in short cadence with a time interval of almost 1 minute. Since we are interested in low frequencies,

long-cadence data are sufficient to capture long period variations. The characteristics of long-cadence data are discussed by Jenkins et al. (2010). Within its orbit of 372.5 d, the *Kepler* space craft performs a 90° roll every 3 months to keep its solar panels aligned with the sun. This resulted into quarters named Q₀ upto Q₁₇. The commissioning run (Q₀) only lasted for 10 days, quarters Q₁ and Q₁₇ were only 1 month long. This study uses the data for all the quarters, unlike in Balona (2013) where only the data from quarters Q₀ to Q₁₂ were available.

The light-curves are stored in the form of a Flexible Image Transport system (FITS) product, which contain tables with a combination of header key words (Borucki et al. 2010; Koch et al. 2010). Among others, the light-curves contain simple aperture photometry (SAP) and pre-search data conditioning (PDC) flux (Thompson et al. 2016). The SAP flux results from the application of the *Kepler* data processing pipeline, which only uses a basic calibration, and is affected by errors. The dominant sources of errors include: differential velocity aberration and thermal transients from the reaction wheel desaturation and quarterly rolls (Smith et al. 2012; Stumpe et al. 2014). The PDC module of the data processing pipeline tries to identify and minimise such signal distortions and noise without jeopardising astrophysical signals (Smith et al. 2012). The most recent version of the pipeline is the multi-scale Maximum A Prior (msMAP) pipeline, and this is the one available through MAST. A more detailed description of the characteristics of PDC flux is found in Stumpe et al. (2012) and Smith et al. (2012). For our purpose, we adopted the PDC flux. The required input for this procedure (barycentric Julian date relative to JD 2 450 000.00 and the PDC flux) were extracted from the FITS files. The time was converted to barycentric Julian date relative to JD 2 454 950.00 while the PDC flux was converted to millimagnitudes. In different quarters, amplitude variations were observed. To obtain an average amplitude, all the data for all the quarters were stringed together to produce a single light-curve. The detailed analysis of the light-curves and the corresponding results are discussed in Section 3.

3 RESULTS AND DISCUSSION

3.1 Rotation frequencies

A precise estimate of the rotation frequency of a star results in a reliable rotational velocity provided that the radius is known. Fig. 2 represents some of the *Kepler* light-curves that we analysed. These light-curves were used to search for amplitude variations. Inspecting the light-curves, they seem to be modulated. The modulation mostly comes from the beating of the plethora of *r*modes. To a lesser extent in such stars, the amplitude modulation could be the result of two or more sinusoids of slightly different frequencies. In addition, we may also not rule out the possibility of having cool backgrounds or close companions responsible for the rotational modulation, though this is expected to be a rare occurrence in our sample. The cooler T_{eff} and greater distance of the background stars would provide weaker total light signal than the study sample. The weaker total light signal would create very small rotational modulation effects

¹ <http://archive.stsci.edu/>

which would not always manifest as a measurable effect in our star's light curve. This implies that the observed signal is intrinsic to the star. The majority of the light-curves display low amplitudes which hampers the visibility of the amplitude variations. An appropriate tool to display and quantify amplitude variability is the discrete Fourier transform for the unequally spaced data (Swan 1982).

For all the stars in our sample, frequencies were calculated from the light-curves using the discrete Fourier fitting technique incorporated in the software package *Period04* (Lenz & Breger 2005). In Fig. 3, we present typical periodograms for selected stars, whose light-curves are shown in Fig. 2. By entirely visual inspection of the periodograms, we identified the frequencies. The features of much interest in the frequency spectra are broad humps of unresolved frequencies coupled with spikes at their slightly higher frequency end. The “hump and spike” features were found in frequency spectra of 131 normal A and 39 Am/Fm stars. Since it is hard to reliably distinguish between true signals and noise at very low frequencies, the part of the periodogram below 0.05 d^{-1} was always ignored. In Fig. 3, the panels on the left show the rotation frequencies ($f_{\text{rot,lit}}$) from the literature (Balona 2013; Balona et al. 2015). The $f_{\text{rot,lit}}$ values correspond to the dominant frequencies in a given periodogram. The middle panels show “hump and spike” features. Features in the right panels correspond to their harmonics. However, in some stars such harmonics are not visible enough, especially for the humps. The presence of harmonics is a characteristic of stellar rotation and the presence of spots. Since the light curve is more of non-sinusoidal shape, the spots create frequency harmonics in the Fourier transform depending on the spot latitude and the inclination angle (Chowdhury et al. 2018).

From the periodograms shown in Fig. 3, spike frequencies were obtained and considered as rotation frequencies (Saio et al. 2018). The results for normal A and Am/Fm stars are depicted in Tables A1 and A2, respectively. The uncertainties in rotation frequencies were computed using the least squares algorithm and found to be of the order of 10^{-5} d^{-1} . In Fig. 4, we compare our rotation frequencies (f_{rot}) and photometric amplitudes (A_{rot}) with values from previous studies, $f_{\text{rot,lit}}$ and $A_{\text{rot,lit}}$, respectively, (Balona 2013) and (Balona et al. 2015). The full black line is the 1:1 relation, and the dashed lines correspond to harmonics (1:N) and sub-harmonics (N:1). For the stars that lie along the line with 1:1 relation, the spike corresponds with the frequency of the highest amplitude in a given periodogram. In such cases, our results are in good agreement with the previous values. For the stars where this is not the case, the corresponding values of rotation frequency and amplitude are different, and the discrepancy increases with increasing N. The residuals in rotation frequencies and amplitudes from the 1:1 lines are represented in panels (b) and (d), respectively. The stars whose rotation frequencies and amplitudes we have entirely corrected lie off the 1:1 line in the panels (a) and (c).

3.2 Rotational velocities

Using the resulting rotation frequencies and stellar radii, rotational velocities were calculated from,

$$V_{\text{rot}} = 2\pi R_{\text{eq}} f_{\text{rot}}, \quad (1)$$

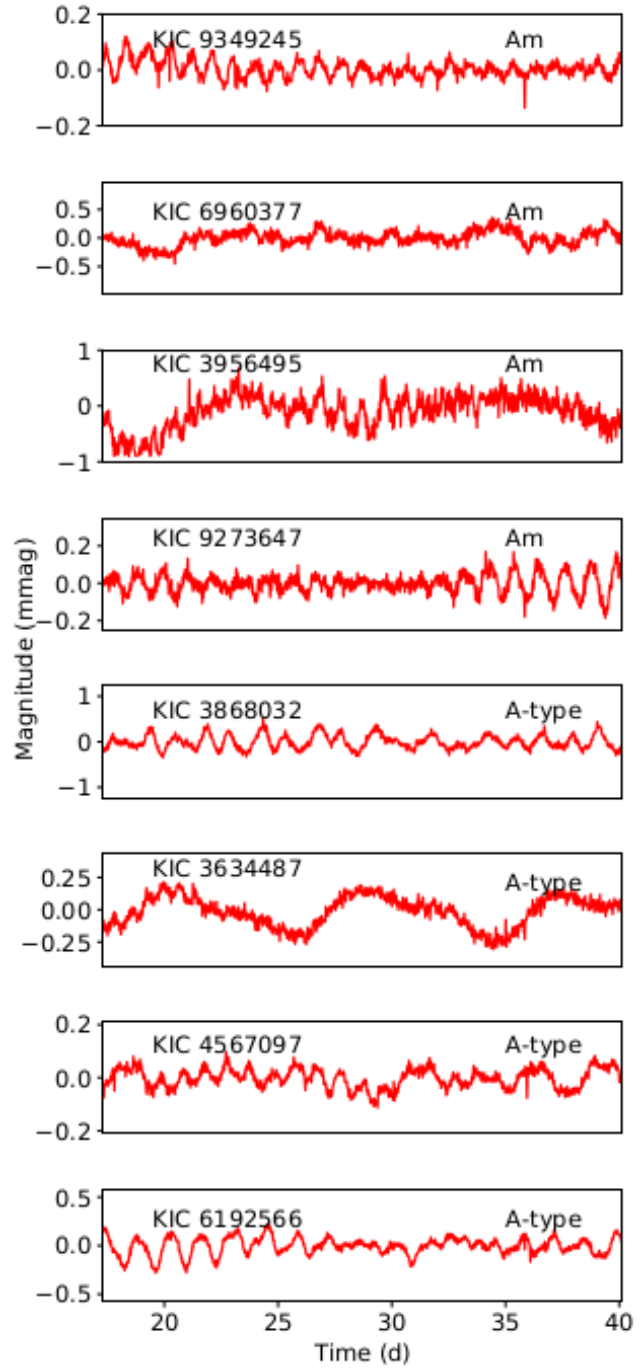


Figure 2. Typical light-curves of Am/Fm and normal A stars in the sample of selected stars.

where V_{rot} is the equatorial rotational velocity in km s^{-1} , R_{eq} is the equatorial stellar radius in km and f_{rot} is the rotation frequency in Hz. We used the mean stellar radius (R) which we calculated from,

$$\log\left(\frac{R}{R_{\odot}}\right) = 0.5\log\left(\frac{L}{L_{\odot}}\right) - 2.0\log(T_{\text{eff}}) + 7.52340473, \quad (2)$$

instead of the R_{eq} . In most cases, R_{eq} is identical to R and the difference does not change the 3σ significance level of the result. We derived the luminosity parameter ($\log(L/L_{\odot})$)

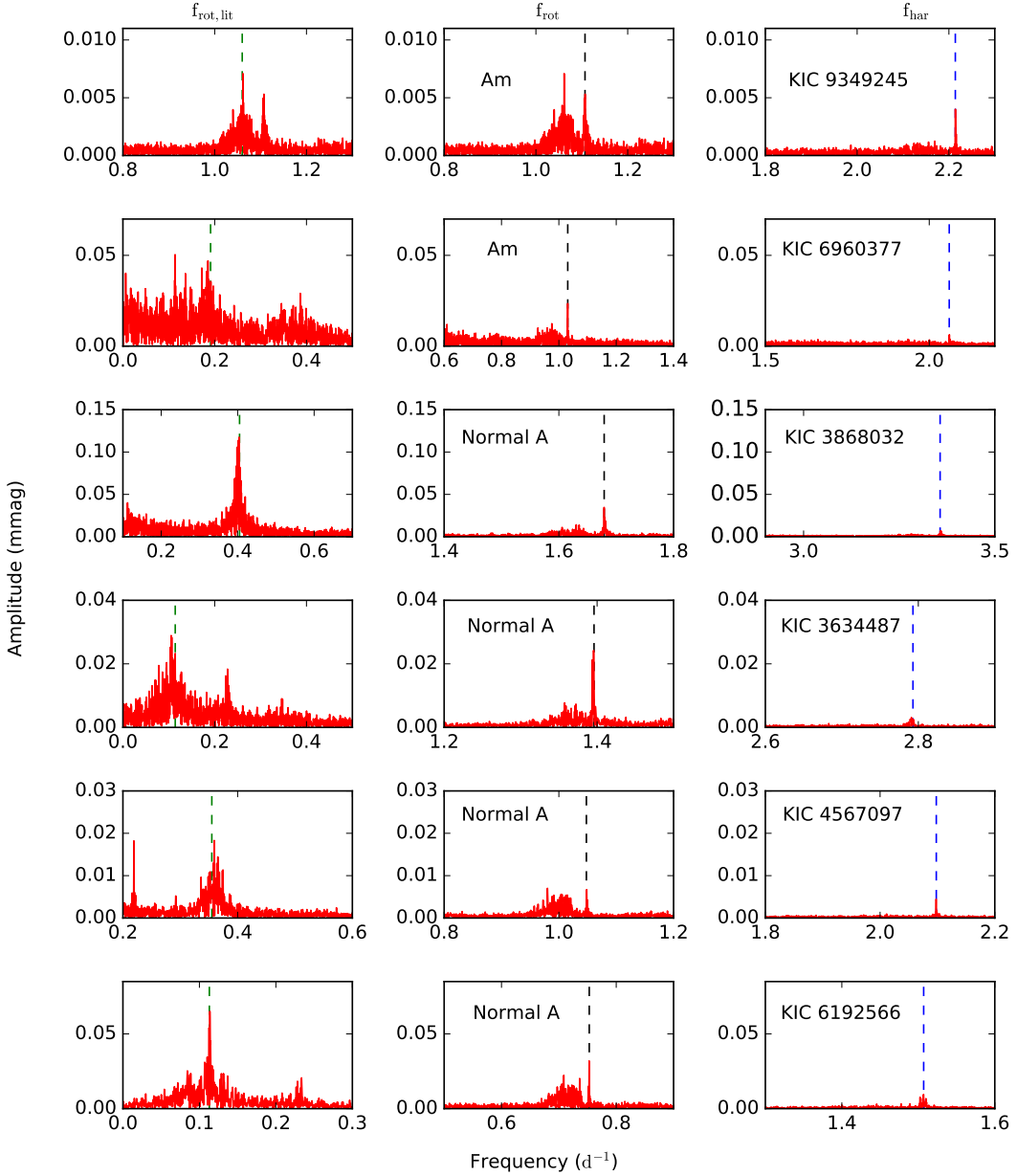


Figure 3. Frequency spectra of selected Am/Fm and normal A stars based on the 4-year *Kepler* data. The green dashed lines in the panels on the left represent the rotation frequencies ($f_{\text{rot}, \text{lit}}$) from the literature (Balona 2013; Balona et al. 2015). Panels in the middle indicate the “humps and spikes” features and those on the right show their first harmonics. The black dashed lines represent the estimated rotation frequencies (f_{rot}) and the blue dashed lines represent the frequency equivalent to $2f_{\text{rot}}$. In the cases where f_{rot} is different from $f_{\text{rot}, \text{lit}}$, the spike is not the dominant frequency on which $f_{\text{rot}, \text{lit}}$ was based.

from GAIA parallaxes (Gaia Collaboration 2018), reddening from a 3D model (Green 2018; Green et al. 2019) and adopted the effective temperature (T_{eff}) from the revised catalog of *Kepler* targets for the Q1–17 by Mathur et al. (2017). For stars whose parallaxes are unknown, we considered the radius from the revised catalog of *Kepler* targets by Mathur et al. (2017). The resulting values for luminosity, stellar radius and rotational velocities for normal A and Am/Fm stars are listed in Tables A1 and A2. In Fig. 5, our derived $\log(L/L_{\odot})$ is compared with that determined by Murphy et al. (2019) for 158 stars that fall on the sample

list of the two studies. The two luminosities agree very well with a correlation coefficient, r , of 0.96.

We calculated the average rotational velocity of Am/Fm and normal A stars as $105 \pm 3 \text{ km s}^{-1}$ and $161 \pm 3 \text{ km s}^{-1}$, respectively. Am/Fm stars rotate slowly relative to normal A stars. This confirms the conclusion from several studies (e.g. Abt & Morrell 1995; Adelman 2004; Stateva et al. 2009; Gebran et al. 2016). For 103 of the “hump and spike” stars in our sample, their projected rotational velocity ($v \sin i$) is available from the LAMOST-*Kepler* project (Frasca et al. 2016) obtained from analysis of low resolution ($\lambda \approx 1800$) spectra using the code ROTFIT (Frasca et al. 2003, 2006).

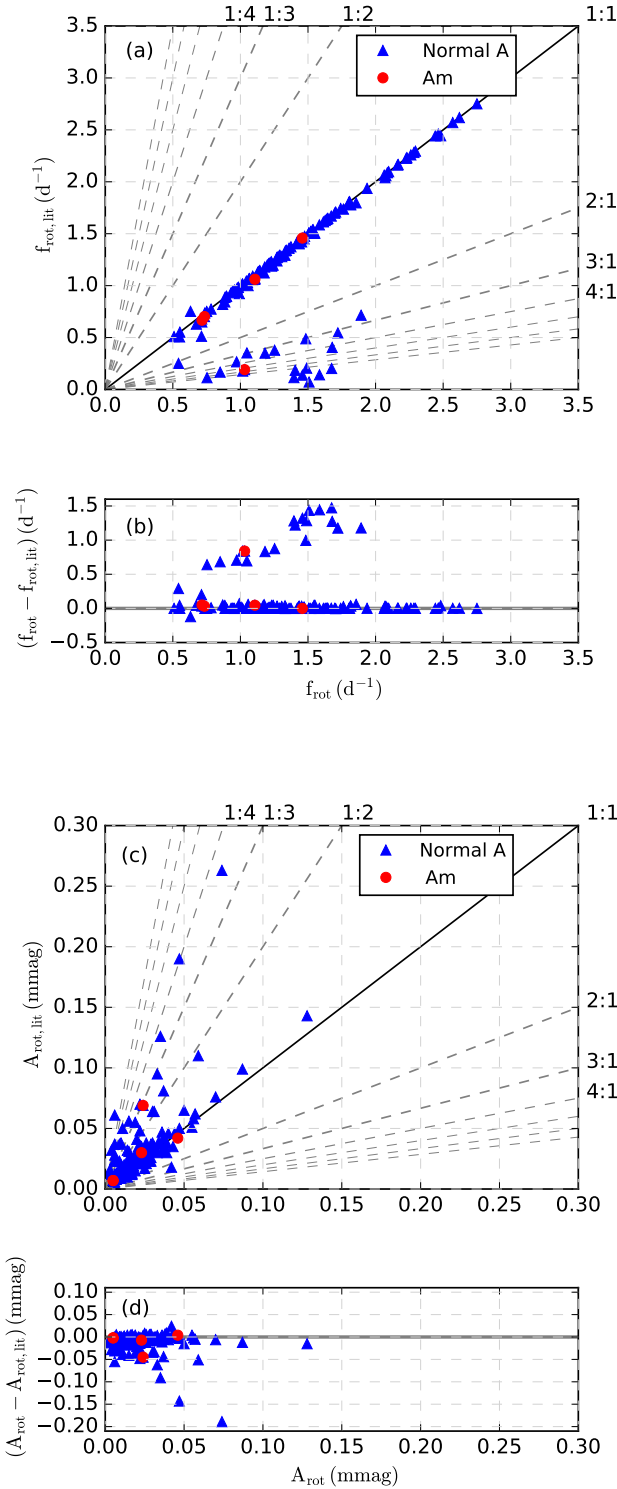


Figure 4. In panel (a), comparison of rotation frequencies (f_{rot}) with values from previous studies ($f_{\text{rot,lit}}$). Panel (b) shows the residuals in the rotation frequencies. In panel (c), photometric amplitudes (A_{rot}) compared with the values ($A_{\text{rot,lit}}$) from the literature (Balona 2013; Balona et al. 2015). Panel (d) represents the residuals in the photometric amplitudes. The full black line is the 1:1 relation, and the dashed lines correspond to harmonics (1:N) and subharmonics (N:1). In panels (a) and (c), the stars that fall off the 1:1 line have rotation frequencies and amplitudes, respectively, which we have completely corrected.

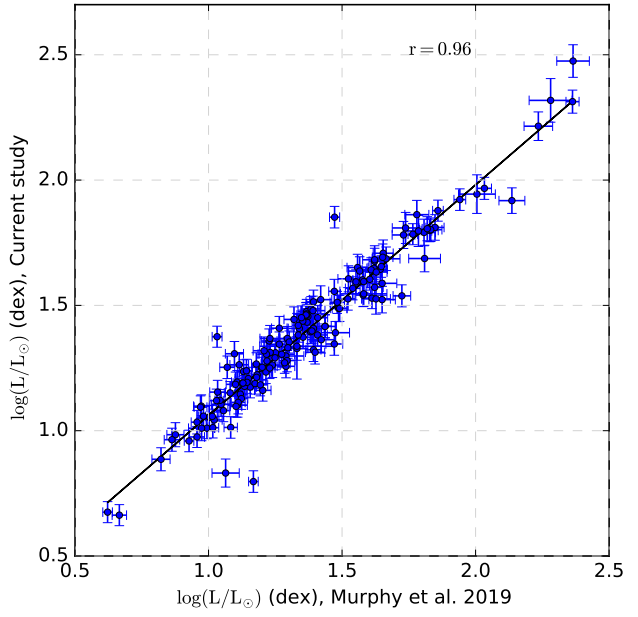


Figure 5. The $\log(L/L_{\odot})$ determined by us compared with that computed by Murphy et al. (2019). The black solid line corresponds to the best fit. r -value the correlation coefficient is given in the top right corner.

For KIC 9117875, KIC 11443271 and KIC 9349245, $v \sin i$ determined from high-resolution spectroscopy by Niemczura et al. (2015), Pedersen et al. (2017) and Niemczura et al. (2017), respectively, was adopted. Given the low resolution of LAMOST spectra, a value of $v \sin i$ below 120 km s^{-1} can not be determined. Therefore, for the stars tagged with “ < 120 ” in column 11 of Tables A1 and A2, we only know that they are rotating slowly in the sense that their $v \sin i$ is below 120 km s^{-1} (Frasca et al. 2016). To validate the V_{rot} determinations, we compared our measurements with the available $v \sin i$ from Niemczura et al. (2015), Frasca et al. (2016), Pedersen et al. (2017) and Niemczura et al. (2017), but ignoring the stars with $v \sin i < 120 \text{ km s}^{-1}$ by Frasca et al. (2016). The results are shown in Fig. 6, where the blue, green and black dashed lines correspond to $i = 90^\circ$, 60° and 30° , respectively, and show the direction a star would move if it had a different inclination. Two stars appear slightly above the line $\sin i = 1.0$ (i.e.; $i = 90^\circ$). However, based on the lower limit of their error bars they fall in the reality zone. This implies that their $v \sin i$ is slightly lower than what is observed. Generally, this is a promising result, though one would get assurance if i was known and $v \sin i$ from high resolution spectroscopy was available for all the stars in our sample. Unfortunately, the majority of the stars in the sample are too faint ($V \geq 11$ mag) to be able to obtain a high-resolution spectrum with a sufficient quality with small (1-2 m) ground-based telescopes.

Fig. 7 shows the distribution of the derived V_{rot} in the current study as compared with the $v \sin i$ for the A-type stars studied by Royer et al. (2007). In their analysis, the authors considered only normal stars of spectral types from B9 to F2. Therefore, for homogeneity, only normal A stars in our sample are included. From Fig. 7, the normal A stars

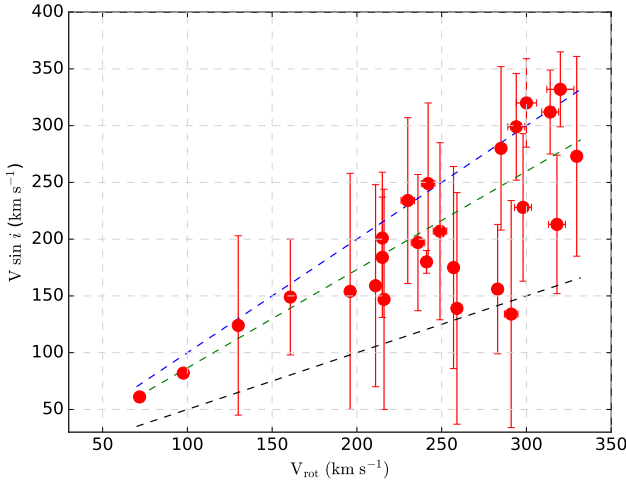


Figure 6. The projected rotational velocity as a function of equatorial rotational velocity. The blue, green and black dashed lines correspond to $i = 90^\circ$, 60° and 30° , respectively.

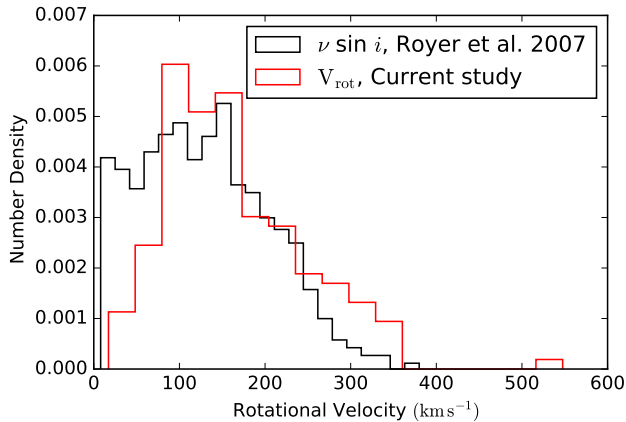


Figure 7. The distribution the equatorial rotational velocity for the normal A stars in the current study and projected rotational velocity, $\nu \sin i$ for A-type stars analysed by Royer et al. (2007).

in our sample have a wide range of rotational velocity which is representative of A stars in general when compared with the distribution of $\nu \sin i$ obtained by Royer et al. (2007).

3.3 Starspot size

The starspot size can give a clue of how strong the magnetic field is on the surface of a star. The knowledge of global magnetic field strength would facilitate giving informative and sound explanations about the development of the chemical peculiarities in intermediate-mass stars since the magnetic field may stabilise against convection which would otherwise hinder atomic diffusion. From the light-curves in Fig. 2 and periodograms in Fig. 3, amplitude variations and frequency spikes were observed. The amplitude variations in the light-curves and the spikes in the frequency spectra could be due to the presence of one or more starspots (Balona 2013; Balona et al. 2015; Saio et al. 2018). The starspot size

can be determined directly from Doppler imaging (Collier Cameron 1995; Barnes et al. 2002).

However, currently there is no direct method for calculating the starspot size photometrically. It has been reported that, within a magnetic cycle, the solar photometric variability increases with the activity levels (Krivova et al. 2003). Assuming that the largest active regions dominate the modulation, as a proxy, the photometric amplitude of the rotation frequency can be extrapolated to be representative of the starspot size (Balona 2013; Giles et al. 2017). The amplitude may not give the exact magnitude of the starspot size but gives a good approximation.

From the frequency spectra, we obtained and considered the amplitudes of the spikes to be the photometric amplitudes (A_{rot}) associated with rotation. The uncertainties in amplitude were calculated using Monte Carlo simulations (Lenz & Breger 2005). The results are listed in Tables A1 and A2. The average A_{rot} of Am/Fm and normal A stars was found to be $\sim 21 \pm 2$ ppm and $\sim 19 \pm 2$ ppm, respectively.

For simplicity, we assume a single, circular and black spot to produce the amplitude of the spike and the stars to be spherical. This is identical to determining the size of an exoplanet from a transit. The radius of the spot (R_{spot}) is given by the standard relation,

$$R_{\text{spot}} = \sqrt{A_{\text{rot}}} R. \quad (3)$$

We estimated the spot radii using Eq. 3, the results are given in column 12 of Tables A1 and A2 and their distribution is shown in Fig. 8. Indeed, the spots maybe regions of a lower T_{eff} (Strassmeier 2009) and hence could appear a little darker instead of completely dark. Considering the T_{eff} of the active region (spot) and the photosphere of the star to be T_{spot} and T_{phot} , respectively, Eq. 3 becomes,

$$R_{\text{spot}} = \sqrt{A_{\text{rot}}} R \left(\frac{T_{\text{phot}}}{T_{\text{spot}}} \right)^2. \quad (4)$$

Strassmeier (2009) reported that the spot-to-photosphere temperature ratio ($T_{\text{spot}}/T_{\text{phot}}$) is about 0.8 for active G and K stars and that, on average, the temperature difference appears to be larger for hotter stars. Therefore, we expect $T_{\text{phot}}/T_{\text{spot}} \geq 1.25$, which translates via Eq. 4 into starspot size that is larger by a factor of ≥ 1.56 (Strassmeier 2009). There is a theoretical evidence that spots originating from ultra-weak magnetic fields might be hotter with a temperature difference of the order of 10 K, and hence only a very small effect on the starspot size (Cantiello & Braithwaite 2019). In addition, the calculated R_{spot} is the starspot group size if there are several spots on the star. The distributions of both normal A and Am/Fm stars are similar and range from 0.2 to about 3.7 R_E , where R_E is the Earth radius. The derived average spot radius is 1.01 ± 0.13 and $1.16 \pm 0.12 R_E$ for Am/Fm and normal A stars, respectively. Generally, the starspot size in normal A and Am/Fm stars is smaller than previously estimated by Balona (2013) and Balona et al. (2015) by about 38 %. This implies that the activity in Am/Fm and normal A stars is weaker than previously suggested by these studies.

3.4 Decay-time scale

The starspot decay-time scale gives a clue of how long the overall starspots are sustained on the stellar surface, once

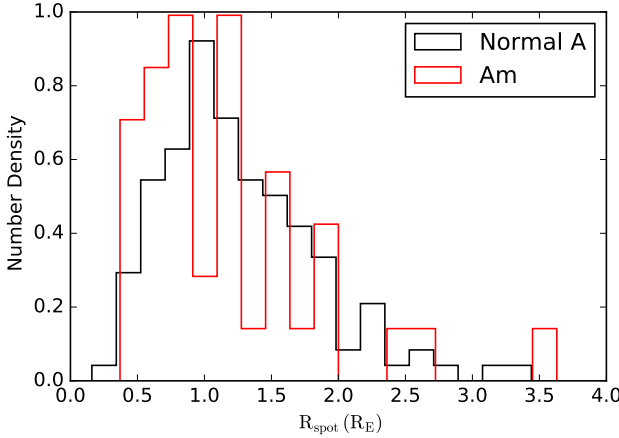


Figure 8. The distribution of the spot size for normal A and Am/Fm stars in our study calculated using Eq. 4.

they have appeared. The rate of starspot growth and decay could be linked to the surface magnetic field strength. The starspot growth and decay contributes to amplitude variations in the light-curves. For a better understanding and explanation of various phenomena observed in normal A and Am/Fm stars, good estimates of the decay-time scale are needed. The decay-time scale was determined from fitting autocorrelation functions (ACFs) of the light-curves. The ACFs show how similar light-curves are to themselves at certain time differences.

For each star, the *Kepler* light-curves from all the available quarters were combined together end-to-end and the resultant light-curve was cross-correlated with itself at a given time lag to produce ACF (McQuillan et al. 2013, 2014). The ACF was normalised on dividing it by the sum of deviations in the flux. For the majority of the stars, the ACFs increase and decrease quasi-sinusoidally depending on the presence of a co-rotating obstacle in the field of view of the star. At time lags greater than zero, the ACF tends to mimic the displacement of an under-damped simple harmonic oscillator (uSHO), (Giles et al. 2017)

$$y(t) = e^{-t/\tau_{DT}} \left(A \cos\left(\frac{2\pi t}{P_{ACF}}\right) + B \cos\left(\frac{4\pi t}{P_{ACF}}\right) + y_0 \right), \quad (5)$$

where

$$t = \Delta T \times n, \quad (6)$$

here t is the time lag in days, ΔT is the median time difference of the light-curve, n ascends from 0 to the total number of ACFs, $y(t)$ is the ACF, τ_{DT} is the decay-time scale of the dominant active region, P_{ACF} is the stellar rotation period, and A , B and y_0 do not represent any physical stellar properties but are constants that are useful in fitting the uSHO equation. All the ACFs were fitted with Eq. 5 using χ^2 minimisation. An example of the ACF for the Am/Fm star KIC 5121064 is given in Fig. 9. The second term in Eq. 5 is significant for this star, inducing subsequent high and low local maxima in the ACF. Indeed, in Fig. 9, the second local maximum corresponds to the rotation period (P_{ACF}) while a lower local maximum is observed at almost half the rotation period. This smaller peak is catered for by the second term

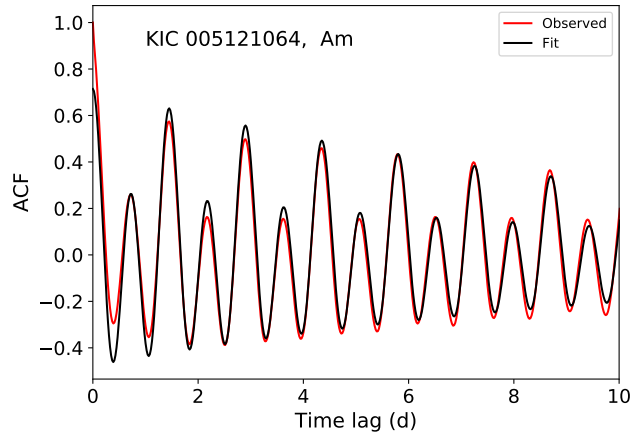


Figure 9. A typical example of autocorrelation function where the second term of Eq. 5 is manifested.

in Eq. 5. An ACF as the one in Fig. 9 indicates that there is(are) weak starspot(s) opposite to the stellar face with the dominant starspot(s). Examples of autocorrelation functions where this scenario is not pronounced are shown in Fig. 10. Inspection of the ACFs was done visually. In general, good quality fits were produced by the least-squares routine (χ^2 minimisation).

About 40% of the ACFs do not show any significant peaks. Examples of such ACFs are shown in Fig. 11, where it is observed that generally the ACF decays instantly without significant local maxima. This points towards a short decay-time and low amplitudes, so it suggests very weak or the absence of starspots and co-rotating structures. However, the “hump and spike” features exist in their frequency spectra. This implies that significantly large starspots may not be required to produce the existing spikes in the frequency spectra. A similar observation was made by Saio et al. (2018) as very small starspots were enough to produce spikes in the models. The resulting values of the decay-time τ_{DT} and the period P_{ACF} are listed in Tables A1 and A2. The stars without any significant peaks in their ACFs have (*) assigned to their τ_{DT} values in the Tables and they were not considered during the discussion of the decay-time scale. In Fig. 12, rotation periods derived from ACFs (P_{ACF}) are compared with periods from the spikes (P_{rot}). The black solid and dashed lines represent the 1:1 relation and the harmonics (1:N) and subharmonics (N:1), respectively. The two periods are well in agreement. However, there are two normal A stars (KIC 4557097 and KIC 10068389) for which the periods of both methods do not agree. This implies that the spikes get overshadowed by the dominant frequencies during the ACF analysis. This is because the spikes are not the dominant peaks in their periodograms. This also applies to all the stars that do not perfectly lie along the line 1:1. We also never considered the two stars (KIC 4557097 and KIC 10068389) in the analysis of the decay-time scale of the sample.

The majority of the stars have decay-time scales of a few days or less, as shown in Fig. 13(e₁₋₃). The average decay-time in Am and normal A stars is 3.6 ± 0.2 and 1.5 ± 0.2 days, respectively. The difference may not be associated with the

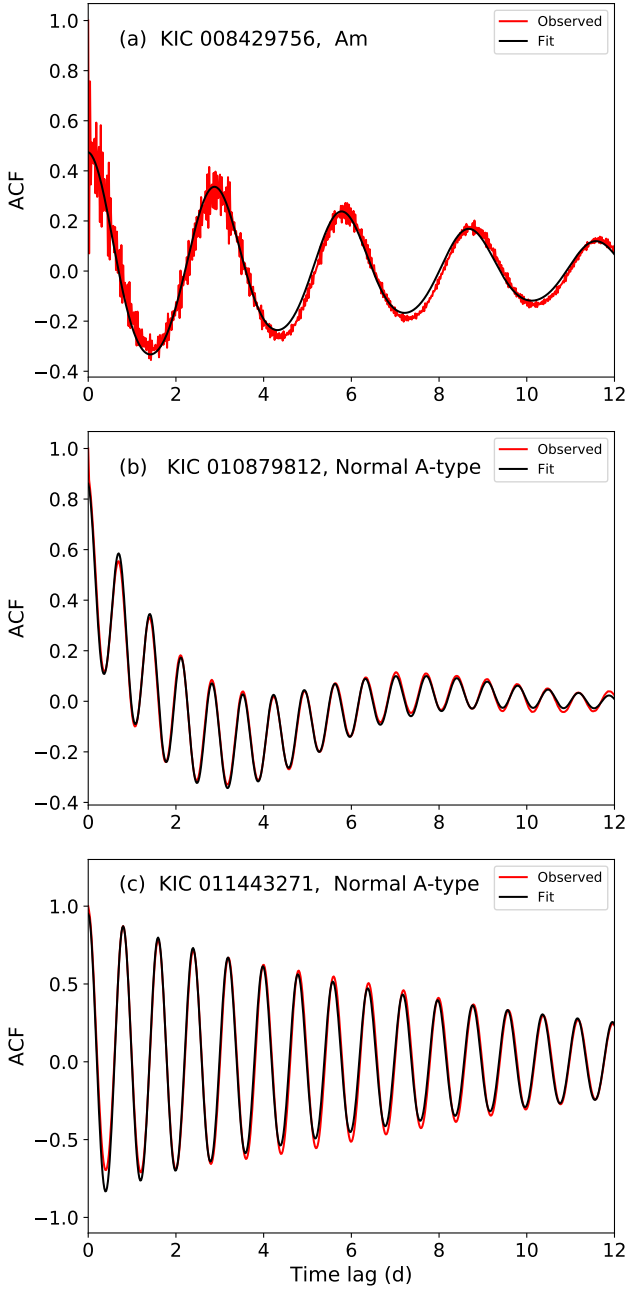


Figure 10. Examples of autocorrelation functions (ACF) plots where the spot(s) is(are) dominant on only one side of the star and so the second term of Eq. 5 is overshadowed. The first peak corresponds to a time lag equivalent to the rotation period.

difference in the rotation velocities between the two groups of stars (discussed in Sect. 3.2), as we observed no correlation between the two parameters. However, the difference could be attributed to the difference in effective temperature. The Am/Fm stars are, in general, cooler than normal A stars in our sample as shown in Fig. 14. The thin convective subsurface layer reduces as the effective temperature increases, which affects the decay lifetime of the available spots. The decay-time scales in Am and normal A indicate that spots in these stars are short-lived compared with those in G, K

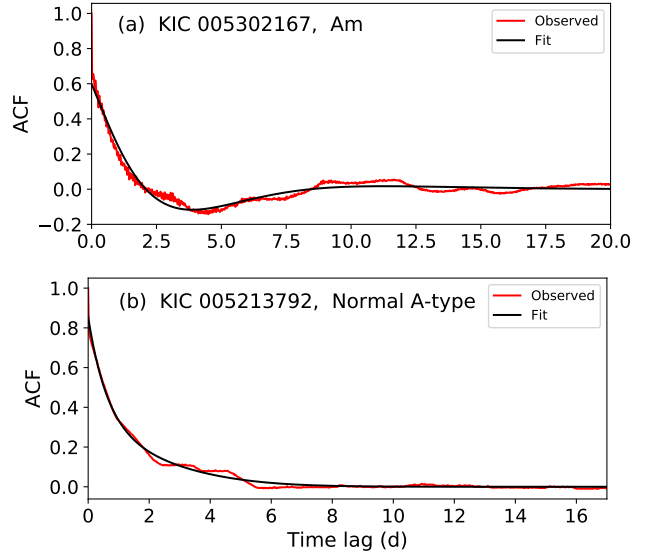


Figure 11. Examples of autocorrelation functions (ACF) which do not show any significant peaks.

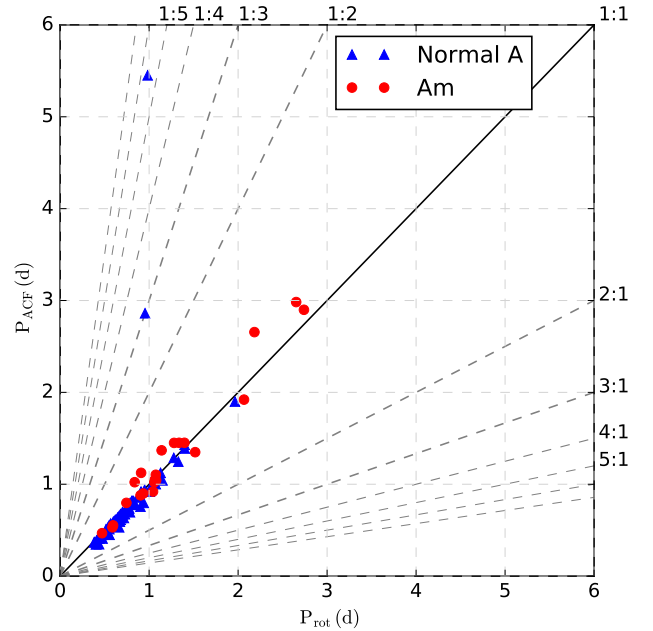


Figure 12. Comparison of rotation periods derived by different methods. The black solid line represents 1:1 relation, while the dashed lines indicate the harmonics (1:N) and subharmonics (N:1). There are two normal A stars with periods that differ a factor of 3 or more.

and M stars. Spots of similar emergence and disappearance time of only a few days were observed in Vega by Petit et al. (2017). The spots in G, K and M stars can stay on the surface for as long as 400 days (Giles et al. 2017). Giles et al. (2017) observed that big starspots live longer on any given star. In Fig. 15, there is a weak positive correlation between spot radius (R_{spot}) and the decay-time scale (τ_{DT}) for the stars in our sample. This implies that the τ_{DT} -values weakly

depend on the spot size in these stars, and a significantly large sample is required to confirm the observation. Giles et al. (2017) also reports that starspots decay more slowly on cooler stars. Normal A and Am/Fm stars are hotter than G, K and M stars, which verifies the observations of short decay-time scale. The observed spot sizes and decay-time scales suggest the presence of a weak magnetic field in the stars of our sample. The magnetic fields could be in the similar range as observed for Vega (Lignières et al. 2009), Sirius (Petit et al. 2011), β UMa and θ Leo (Blazère et al. 2014), HD 188774 (Neiner & Lampens 2015), Alhena (Blazère et al. 2016a) and ρ Pup (Neiner et al. 2017). Cantiello & Braithwaite (2019) reported a similar suggestion that, except for the Ap stars, the other main sequence A-type stars can have magnetic fields of a few Gauss. Some studies show that such magnetic field can support weak starspots (e.g; Blazère et al. 2016a; Neiner et al. 2017; Cantiello & Braithwaite 2019). Nevertheless, we may not rule out the possibility of the observed spots having an origin other than the magnetic fields that is still unknown.

3.5 Correlation of rotation and spot properties with other parameters

This study presents a detailed analysis of the rotation properties of “hump and spike” stars. We analysed *Kepler* photometric data of 170 stars. The distribution of the rotation properties of our sources over the temperature (T_{eff}), surface gravity ($\log g$) and luminosity ($\log(L/L_{\odot})$) domains is represented in Fig. 13. Panels (a₁₋₃), (b₁₋₃), (c₁₋₃), (d₁₋₃) and (e₁₋₃) of Fig. 13 show how f_{rot} , V_{rot} , A_{rot} , R_{spot} and τ_{DT} , respectively, vary with the T_{eff} , $\log g$ and $\log(L/L_{\odot})$ of the studied stars. From panels (a₁) and (b₁), rotation frequency and velocity are moderately correlated with effective temperature. The A_{rot} (panel (c₁)) and spot radius (panel (d₁)) have no significant relation with T_{eff} for these stars. A weak dependence of τ_{DT} on T_{eff} is observed in panel (e₁). A similar observation is reported by Giles et al. (2017) for the G, K and M stars. From the panels in the middle, the rotation and spot properties are independent of $\log g$ for these stars. Based on the r-values in panels (a₃) and (d₃), the rotation frequency and the spot size weakly depend on luminosity. Panel (b₃) indicates a moderately strong relation between V_{rot} and $\log(L/L_{\odot})$. There is no dependence of A_{rot} and τ_{DT} on $\log(L/L_{\odot})$ for these stars. From panels (c₁₋₃), (d₁₋₃) and (e₁₋₃), we conclude that in general, the photometric amplitudes, spot radii and spot decay-time scales of normal A and Am/Fm stars are on average 0.025 mmag, 1.61 R_E and 3.3 days, respectively.

Fig. 16 shows distribution of the rotation and spot properties in the Hertzsprung-Russell diagram. The majority of the stars are beyond the blue edge of the theoretical δ Scuti instability strip calculated by Dupret et al. (2004). In Fig. 16(a) and (b), the rotation frequency and velocity increase with towards the more massive stars, while the spot radius, in panel (d), seem to increase as stars move off the zero age main sequence. There are no observable patterns for photometric amplitude and decay-time scale in panels (c) and (e), respectively. The observations will be confirmed when a significantly large number of stars is used. Efforts are being made to search for “hump and spike” stars in the K2 and *TESS* archives.

The magnetic field in all the stars in the sample is presumed ultra weak and magnetic braking may not explain the observed trend of rotation properties. As we ascend the main sequence the effective temperature, luminosity and mass increase. The more massive stars rotate faster because they have higher initial angular momenta (Bouvier 2013).

4 CONCLUSION

The rotation frequencies of both normal A and Am/Fm stars were obtained from their frequency spectra using “hump and spike” features. Rotation frequency and velocity are found to depend moderately on T_{eff} . A good agreement between the rotational velocities and the available $v \sin i$ from the literature was observed. However, a comparison of the two velocities would be more feasible if $v \sin i$ from high-resolution spectroscopy was available and i was known. The photometric amplitudes were determined and used as proxies for the size of the starspots. The average photometric amplitude of Am/Fm and normal A stars was found to be $\sim 21 \pm 2$ ppm and $\sim 19 \pm 2$ ppm, respectively. After assuming a single, circular and black spot to produce the amplitude of the spike, the average spot radius was found to be 1.01 ± 0.13 and $1.16 \pm 0.12 R_E$ for Am/Fm and normal A stars, respectively. These results indicate that spots in normal A and Am/Fm stars are significantly smaller compared to the previously estimated sizes, 541 ± 86 ppm for normal A and 93 ± 25 ppm for Am/Fm stars by Balona (2013) and Balona et al. (2015), respectively. However, based on the limitations discussed in Sect. 3.3, our analysis gives the lower limit of the spot sizes.

By fitting the autocorrelation functions of the light-curves with appropriate models, no peaks were observed in the ACFs of some stars, a phenomenon that suggests the absence of repeated patterns in their light-curves, and hence of co-rotating structures (starspots). Since such stars have “hump and spike” features in the periodograms, starspots may not be a major requirement to produce spikes in frequency spectra. Based on our R_{spot} values and absence of peaks in the 40 % of the ACFs, spots in most normal A and Am/Fm stars could be very weak or actually absent.

The lifetime of the starspots were found to be in the order of a few days. The sizes of the spots in normal A and Am/Fm stars are in general very similar. In comparison with G, K, and M stars, the spots in normal A and Am/Fm stars are short-lived. This is attributed to the much thinner outer convective zone in normal A and Am/Fm than in G, K, and M stars.

In the next paper of the series, we shall present the high-resolution spectroscopic analysis of a number of “hump and spike” stars observed from La Palma using High-Efficiency and high-Resolution Mercator Echelle Spectrograph (HERMES). In the near future, we also intend to make follow-up studies for K2 and *TESS* targets showing “hump and spike” features in their frequency spectra.

ACKNOWLEDGEMENT

The International Science Program (ISP) of Uppsala University financed the study. The part of work presented

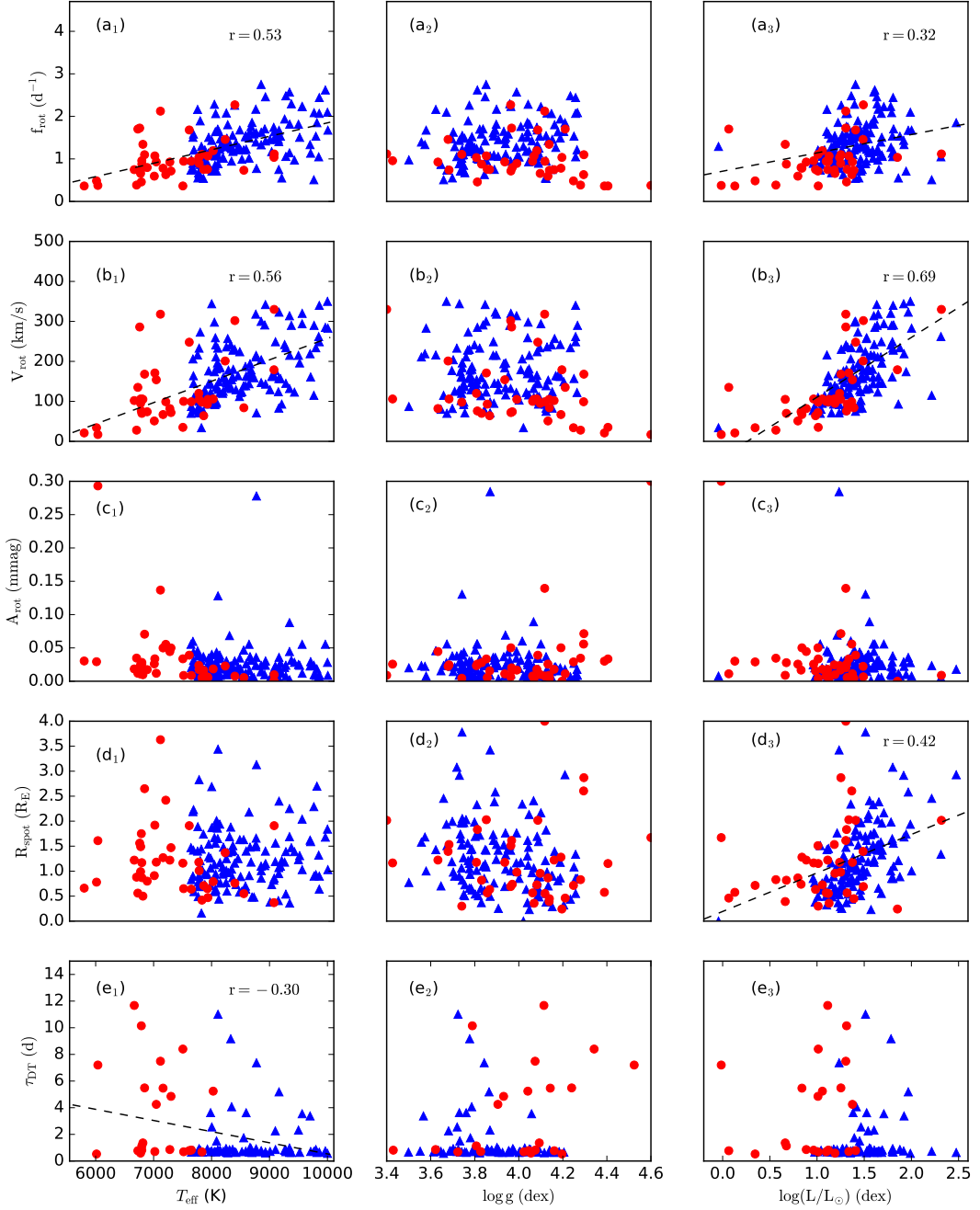


Figure 13. The rotation frequency (a₁₋₃), rotational velocity (b₁₋₃), photometric amplitude (c₁₋₃), spot radius (d₁₋₃) and starspot decay life-time (e₁₋₃) versus effective temperature, surface gravity and luminosity. The T_{eff} and $\log g$ -values from the revised catalog of *Kepler* targets for the Q₁₋₁₇ (DR25) (Mathur et al. 2017) were adopted. The red dots represent Am/Fm stars and blue triangles are normal A stars. The black dashed lines indicate the fits between the respective parameters and the value of the correlation coefficient (r) is given in the top right corner.

here is supported by the Belgo-Indian Network for Astronomy & Astrophysics (BINA), approved by the International Division, Department of Science and Technology (DST, Govt. of India; DST/INT/Belg/P-02) and the Belgian Federal Science Policy Office (BELSPO, Govt. of Belgium; BL/33/IN12). This paper includes data collected by the Kepler mission that were obtained from the Mikulski Archive for Space Telescopes (MAST). The authors thank Professor Donald W. Kurtz and Professor Luis A. Balona

for the discussions and suggestions regarding this work. OT and EJ acknowledge the hospitality given by ARIES during their research visit to initiate the collaboration between ARIES, India and Mbarara University of Science and Technology, Uganda. We acknowledge the anonymous reviewer for his/her careful reading of our manuscript and many insightful comments and suggestions which improved the paper.

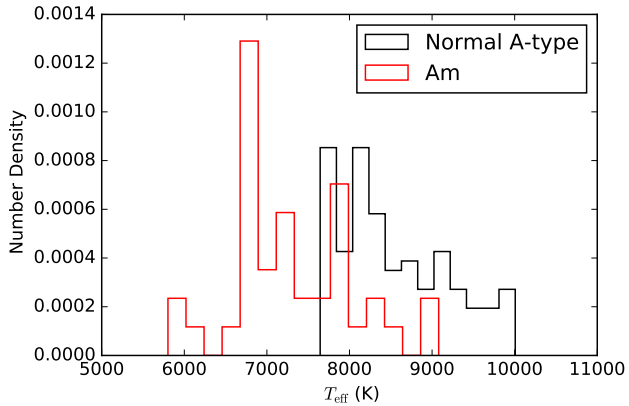


Figure 14. The distribution of the effective temperature for normal A and Am/Fm stars in our study.

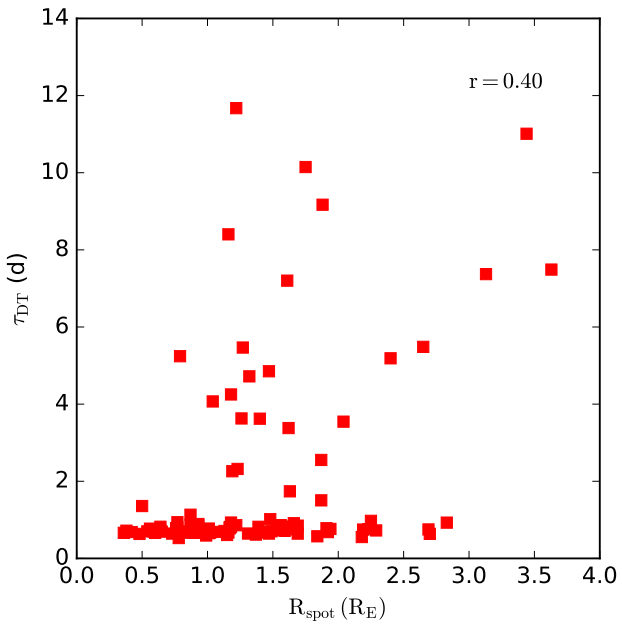


Figure 15. The correlation between the spot radius (R_{spot}) and the decay-time scale (τ_{DT}) for normal A and Am/Fm stars. The black dashed line shows the fit. r -value the correlation coefficient is given at the top right corner.

REFERENCES

- Abt H. A., 1961, *ApJS*, **6**, 37
 Abt H. A., 2009, *AJ*, **138**, 28
 Abt H. A., Morrell N. I., 1995, *ApJS*, **99**, 135
 Adelman S. J., 1986, *A&AS*, **64**, 173
 Adelman S. J., 2004, in Zverko J., Ziznovsky J., Adelman S. J., Weiss W. W., eds, IAU Symposium Vol. 224, The A-Star Puzzle. pp 1–11, doi:10.1017/S1743921304004314
 Ashoka B. N., et al., 2000, Bulletin of the Astronomical Society of India, **28**, 251
 Aurière M., et al., 2007, *A&A*, **475**, 1053
 Aurière M., et al., 2010, *A&A*, **523**, A40
 Balona L. A., 2012, *MNRAS*, **423**, 3420
 Balona L. A., 2013, *MNRAS*, **431**, 2240

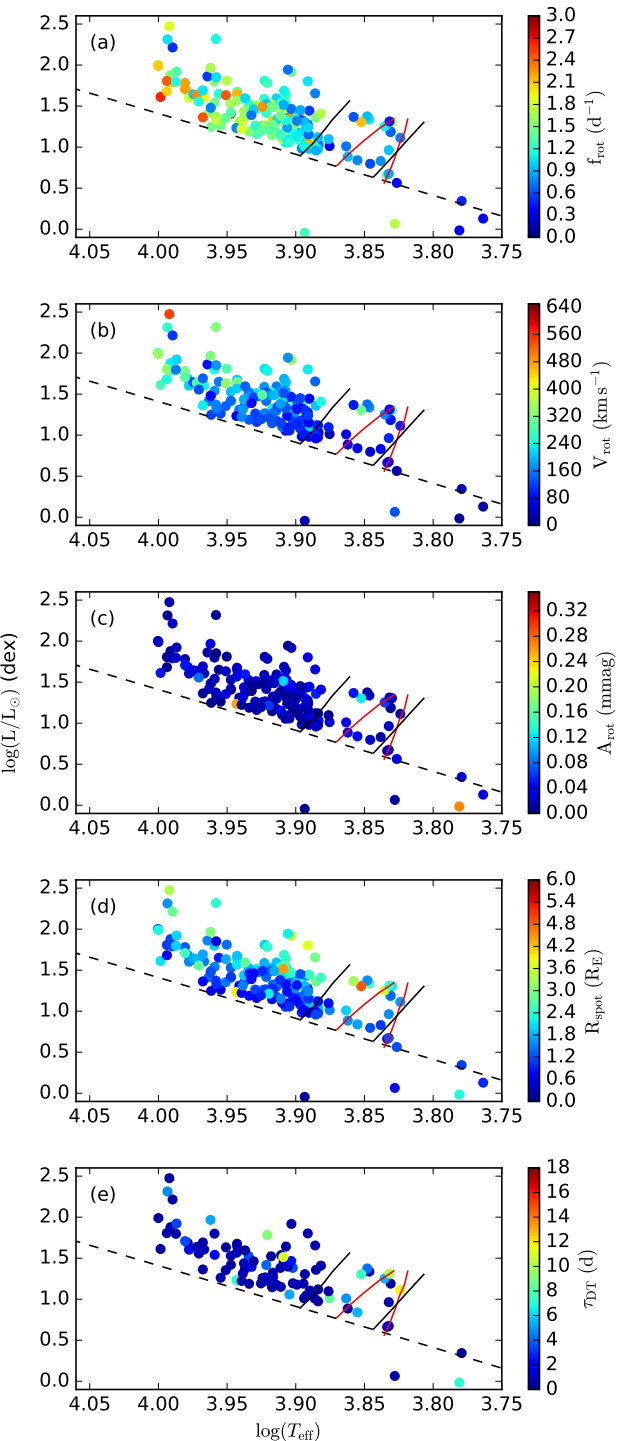


Figure 16. The distribution of the rotation and spot properties in the Hertzsprung-Russell diagram. The black dashed line represents the zero age main sequence. The black and red solid lines indicate the theoretical δ Scuti and γ Doradus instability strips, respectively, as calculated by Dupret et al. (2004).

- Balona L. A., 2014, *MNRAS*, **441**, 3543
 Balona L. A., et al., 2011, *MNRAS*, **414**, 792
 Balona L. A., Catanzaro G., Abedigamba O. P., Ripepi V., Smalley B., 2015, *MNRAS*, **448**, 1378
 Balona L. A., Švanda M., Karlický M., 2016, *MNRAS*, **463**, 1740
 Barnes J. R., James D. J., Collier Cameron A., 2002, *Astronomische Nachrichten*, **323**, 333
 Blazère A., et al., 2014, *Proceedings of the International Astronomical Union*, **10**, 67–72
 Blazère A., Neiner C., Petit P., 2016a, *MNRAS*, **459**, L81
 Blazère A., et al., 2016b, *A&A*, **586**, A97
 Boesgaard A. M., Tripicco M. J., 1986, *ApJ*, **303**, 724
 Borucki W. J., et al., 2010, *Science*, **327**, 977
 Bouvier J., 2013, in Hennebelle P., Charbonnel C., eds, EAS Publications Series Vol. 62, EAS Publications Series. pp 143–168 ([arXiv:1307.2891](https://arxiv.org/abs/1307.2891)), doi:10.1051/eas/1362005
 Braithwaite J., 2014, in Petit P., Jardine M., Spruit H. C., eds, IAU Symposium Vol. 302, Magnetic Fields throughout Stellar Evolution. pp 255–264 ([arXiv:1312.4755](https://arxiv.org/abs/1312.4755)), doi:10.1017/S1743921314002221
 Brandenburg A., 2000, in Cheng K. S., Chau H. F., Chan K. L., Leung K. C., eds, Astrophysics and Space Science Library Vol. 254, ASSL. p. 1, doi:10.1007/978-94-010-0878-5_1
 Browning M. K., Brun A. S., Toomre J., 2004, *ApJ*, **601**, 512
 Cantiello M., Braithwaite J., 2019, *ApJ*, **883**, 106
 Chowdhury S., Joshi S., Engelbrecht C. A., De Cat P., Joshi Y. C., Paul K. T., 2018, *Ap&SS*, **363**, 260
 Claverie A., Isaak G. R., McLeod C. P., van der Raay H. B., Roca Cortes T., 1981, *Nature*, **293**, 443
 Collier Cameron A., 1995, *MNRAS*, **275**, 534
 Conti P. S., 1970, *PASP*, **82**, 781
 Costa G., Girardi L., Bressan A., Marigo P., Rodrigues T. S., Chen Y., Lanza A., Goudfrooij P., 2019, *MNRAS*, **485**, 4641
 De Cat P., et al., 2015, *ApJS*, **220**, 19
 Debernardi Y., 2000, in IAU Symposium. p. 161
 Dupret M. A., Grigahcène A., Garrido R., Gabriel M., Scuflaire R., 2004, *A&A*, **414**, L17
 Dziembowski W., Krolikowska M., Kosovichev A., 1988, *Acta Astron.*, **38**, 61
 Fossati L., Bagnulo S., Landstreet J., Wade G., Kochukhov O., Monier R., Weiss W., Gebran M., 2008, *A&A*, **483**, 891
 Fossati L., Ryabchikova T., Bagnulo S., Alecian E., Grunhut J., Kochukhov O., Wade G., 2009, *A&A*, **503**, 945
 Frasca A., Alcalá J. M., Covino E., Catalano S., Marilli E., Paladino R., 2003, *A&A*, **405**, 149
 Frasca A., Guillout P., Marilli E., Freire Ferrero R., Biazzo K., Klutsch A., 2006, *A&A*, **454**, 301
 Frasca A., et al., 2016, *A&A*, **594**, A39
 Gaia Collaboration 2018, VizieR Online Data Catalog, p. I/345
 Gebran M., Farah W., Paletou F., Monier R., Watson V., 2016, *A&A*, **589**, A83
 Giampapa M. S., Rosner R., 1984, *ApJ*, **286**, L19
 Giles H. A. C., Collier Cameron A., Haywood R. D., 2017, *MNRAS*, **472**, 1618
 Gray R. O., et al., 2016, *AJ*, **151**, 13
 Green G. M., 2018, *JOSS*, **3**, 695
 Green G. M., Schlafly E. F., Zucker C., Speagle J. S., Finkbeiner D. P., 2019, arXiv e-prints, p. arXiv:1905.02734
 Howell S. B., et al., 2014, *PASP*, **126**, 398
 Hui-Bon-Hoa A., 2000, *A&AS*, **144**, 203
 Jenkins J. M., et al., 2010, *ApJ*, **713**, L120
 Joshi S., et al., 2003, *MNRAS*, **344**, 431
 Joshi S., Mary D. L., Martinez P., Kurtz D. W., Girish V., Seetha S., Sagar R., Ashoka B. N., 2006, *A&A*, **455**, 303
 Joshi S., Mary D. L., Chakradhari N. K., Tiwari S. K., Billaud C., 2009, *A&A*, **507**, 1763
 Joshi S., Ryabchikova T., Kochukhov O., Sachkov M., Tiwari S. K., Chakradhari N. K., Piskunov N., 2010, *MNRAS*, **401**, 1299
 Joshi S., et al., 2012, *MNRAS*, **424**, 2002
 Joshi S., et al., 2016, *A&A*, **590**, A116
 Joshi S., Semenko E., Moiseeva A., Sharma K., Joshi Y. C., Sachkov M., Singh H. P., Yerra B. K., 2017, *MNRAS*, **467**, 633
 Kaler J. B., 1989, Stars and their spectra. an introduction to spectral sequence
 Khalack V. R., LeBlanc F., 2015, Advances in Astronomy and Space Physics, **5**, 3
 Khokhlova V. L., 1981, in Liege International Astrophysical Colloquia. pp 457–463
 Koch D. G., et al., 2010, *ApJL*, **713**, L79
 Krivova N. A., Solanki S. K., Fligge M., Unruh Y. C., 2003, *A&A*, **399**, L1
 Kron G. E., 1947, *PASP*, **59**, 261
 Kunzli M., North P., 1998, *A&AS*, **127**, 277
 Lenz P., Breger M., 2005, *CoAst*, **146**, 53
 Lignières F., Petit P., Böhm T., Aurière M., 2009, *A&A*, **500**, L41
 Martinez P., et al., 2001, *A&A*, **371**, 1048
 Mathur S., et al., 2017, *ApJS*, **229**, 30
 McQuillan A., Aigrain S., Mazeh T., 2013, *MNRAS*, **432**, 1203
 McQuillan A., Mazeh T., Aigrain S., 2014, *ApJS*, **211**, 24
 Michaud G., 1970, *ApJ*, **160**, 641
 Monier R., 2019, *Research Notes of the AAS*, **3**, 118
 Mosser B., Baudin F., Lanza A. F., Hulot J. C., Catala C., Baglin A., Auvergne M., 2009, *A&A*, **506**, 245
 Mullan D. J., 1973, *Irish Astronomical Journal*, **11**, 32
 Murphy S. J., 2014, PhD thesis, Jeremiah Horrocks Institute, University of Central Lancashire, Preston, UK <EMAIL>murphy@physics.usyd.edu.au</EMAIL>
 Murphy S. J., Hey D., Van Reeth T., Bedding T. R., 2019, *MNRAS*, **485**, 2380
 Neiner C., Lampens P., 2015, *MNRAS*, **454**, L86
 Neiner C., Wade G. A., Sikora J., 2017, *MNRAS*, **468**, L46
 Niemczura E., et al., 2015, *MNRAS*, **450**, 2764
 Niemczura E., et al., 2017, *MNRAS*, **470**, 2870
 North P., Ginestet N., Carquillat J.-M., Carrier F., Udry S., 1998, Contributions of the Astronomical Observatory Skalnate Pleso, **27**, 179
 Noyes R. W., Hartmann L. W., Baliunas S. L., Duncan D. K., Vaughan A. H., 1984, *ApJ*, **279**, 763
 Papaloizou J., Pringle J. E., 1978, *MNRAS*, **182**, 423
 Pedersen M. G., Antoci V., Korhonen H., White T. R., Jessen-Hansen J., Lehtinen J., Nikbakht S., Viuho J., 2017, *MNRAS*, **466**, 3060
 Petit P., et al., 2010, *A&A*, **523**, A41
 Petit P., et al., 2011, *A&A*, **532**, L13
 Petit P., et al., 2014, *A&A*, **568**, C2
 Petit P., Hébrard E. M., Böhm T., Folsom C. P., Lignières F., 2017, *MNRAS*, **472**, L30
 Power J., Wade G. A., Hanes D. A., Aurier M., Silvester J., 2007, in Romanyuk I. I., Kudryavtsev D. O., Neizvestnaya O. M., Shapoval V. M., eds, Physics of Magnetic Stars. p. 89 ([arXiv:astro-ph/0612557](https://arxiv.org/abs/astro-ph/0612557))
 Preston G. W., 1974, *ARA&A*, **12**, 257
 Renson P., 1988, *A&AS*, **76**, 127
 Ricker G. R., et al., 2014, *JATIS*, **1**, 14003
 Royer F., Zorec J., Gómez A. E., 2007, *A&A*, **463**, 671
 Ryabchikova T., Piskunov N., Kochukhov O., Tsymbal V., Mittermayer P., Weiss W. W., 2002, *A&A*, **384**, 545
 Saio H., 1981, *ApJ*, **244**, 299
 Saio H., Kurtz D. W., Murphy S. J., Antoci V. L., Lee U., 2018, *MNRAS*, **474**, 2774
 Sills A., Deliyannis C. P., 2000, *ApJ*, **544**, 944
 Smalley B., et al., 2014, *A&A*, **564**, A69
 Smith J. C., et al., 2012, *PASP*, **124**, 1000

- Soufi F., Goupil M. J., Dziembowski W. A., 1998, *A&A*, **334**, 911
 Stateva I. K., Iliev I. K., Budaj J., Barzova I. S., 2009, *BAJ*, **12**,
 29
 Strassmeier K. G., 2009, *The Astronomy and Astrophysics Review*, **17**, 251
 Stumpe M. C., et al., 2012, *PASP*, **124**, 985
 Stumpe M. C., Smith J. C., Catanzarite J. H., Van Cleve J. E.,
 Jenkins J. M., Twicken J. D., Girouard F. R., 2014, *PASP*,
 126, 100
 Swan P. R., 1982, *AJ*, **87**, 1608
 Takeda Y., Han I., Kang D.-I., Lee B.-C., Kim K.-M., 2008, *Journal of Korean Astronomical Society*, **41**, 83
 Théado S., Vauclair S., Alecian G., LeBlanc F., 2011, in Alecian
 G., Belkacem K., Samadi R., Valls-Gabaud D., eds, SF2A-
 2011: Proceedings of the Annual meeting of the French Society
 of Astronomy and Astrophysics. pp 253–256
 Thompson S. E., Fraquelli D., Van Cleve J. E., Caldwell D. A.,
 2016, Technical report, Kepler Archive Manual
 Turcotte S., 2001, arXiv e-prints, [pp astro-ph/0111179](#)
 Turcotte S., 2003, in Balona L. A., Henrichs H. F., Medupe R.,
 eds, Astronomical Society of the Pacific Conference Series
 Vol. 305, Magnetic Fields in O, B and A Stars: Origin and
 Connection to Pulsation, Rotation and Mass Loss. p. 199
 ([arXiv:astro-ph/0304424](#))
 Vauclair G., 1976, *A&A*, **50**, 435
 Watson W. D., 1970, *ApJL*, **162**, L45

APPENDIX A: TABLES

Table A1. List of normal A stars with “hump and spike” features in their frequency spectra. We list the rotation frequency (f_{rot}), rotational velocity (V_{rot}), rotation frequency amplitude (A_{rot}), frequency of the first harmonic of the rotation frequency (f_{har}) and its amplitude (A_{har}) as derived from their frequency spectra, the effective temperature (T_{eff}) and surface gravity ($\log g$) as reported by Mathur et al. (2017), the luminosity ($\log(L/L_{\odot})$) as derived from Gaia parallaxes (Gaia Collaboration 2018), the stellar radius (R) as estimated from the effective temperature and luminosity, the projected rotational velocity ($v \sin i$) as found in the literature (Frasca et al. 2016) in general; Pedersen et al. (2017) for KIC 11443271, the spot radius (R_{spot}) as estimated from the photometric amplitude, the rotation period (P_{ACF}) and decay-time scale of the starspots (τ_{DT}) as estimated from the autocorrelation functions of their light-curves. (*) marks doubtful measurements.

KIC	f_{rot}	A_{rot}	f_{har}	A_{har}	T_{eff}	$\log g$	$\log(L/L_{\odot})$	R	V_{rot}	$v \sin i$	R_{spot}	P_{ACF}	τ_{DT}
	(d $^{-1}$)	(mmag)	(d $^{-1}$)	(mmag)	(K)	(dex)	(dex)	(R $_{\odot}$)	(km s $^{-1}$)	(km s $^{-1}$)	(R $_{\text{E}}$)	(d)	(d)
1873552	1.21230	0.013 ± 0.002	2.40525	0.004 ± 0.002	7884 ± 83	3.804 ± 0.152	1.080 ± 0.044	1.86 ± 0.06	114 ± 1	< 120	0.73 ± 0.11	-	2.923 (*)
2157489	0.73666	0.051 ± 0.002	1.47356	0.007 ± 0.002	7645 ± 270	3.660 ± 0.275	1.034 ± 0.047	1.88 ± 0.14	70 ± 1	< 120	1.47 ± 0.12	-	1.819 (*)
2158190	1.01611	0.019 ± 0.002	2.03147	0.005 ± 0.001	8204 ± 294	3.723 ± 0.271	1.594 ± 0.048	3.11 ± 0.23	156 ± 2	< 120	1.48 ± 0.14	-	0.699 (*)
3222104	1.26946	0.020 ± 0.001	2.53910	0.007 ± 0.001	8457 ± 318	4.121 ± 0.142	1.475 ± 0.049	2.55 ± 0.20	164 ± 2	< 120	1.25 ± 0.12	-	3.285 (*)
3337124	1.10823	0.022 ± 0.001	2.21620	0.004 ± 0.001	7982 ± 81	3.909 ± 0.135	1.194 ± 0.046	2.07 ± 0.06	116 ± 1	< 120	1.01 ± 0.11	0.756 ± 0.110	0.687 ± 0.108
3634487	1.39543	0.022 ± 0.001	2.79097	0.003 ± 0.001	8765 ± 344	3.552 ± 0.331	1.676 ± 0.052	2.99 ± 0.24	211 ± 3	< 120	1.53 ± 0.13	0.633 ± 0.112	0.735 ± 0.109
3766112	2.23214	0.011 ± 0.001	4.46765	0.005 ± 0.001	9564 ± 644	3.931 ± 0.231	1.781 ± 0.054	2.84 ± 0.38	320 ± 8	332 ± 33	1.03 ± 0.14	-	0.655 (*)
3848948	1.28684	0.020 ± 0.001	2.57368	0.002 ± 0.001	8201 ± 293	3.693 ± 0.290	1.174 ± 0.043	1.92 ± 0.14	125 ± 2	-	0.94 ± 0.12	0.736 ± 0.112	0.726 ± 0.108
3868032	1.67889	0.032 ± 0.002	3.35711	0.006 ± 0.002	8487 ± 318	4.042 ± 0.160	1.512 ± 0.044	2.64 ± 0.20	224 ± 3	-	1.63 ± 0.12	-	7.578 (*)
4059089	2.62009	0.051 ± 0.001	5.23999	0.012 ± 0.001	9964 ± 83	3.789 ± 0.210	1.612 ± 0.047	2.15 ± 0.05	285 ± 2	280 ± 72	1.68 ± 0.11	0.368 ± 0.100	0.753 ± 0.108
4481029	1.45328	0.004 ± 0.001	2.91331	0.001 ± 0.001	9009 ± 81	3.878 ± 0.138	1.262 ± 0.050	1.76 ± 0.05	129 ± 1	< 120	0.38 ± 0.11	0.633 ± 0.105	0.718 ± 0.108
4488313	1.19864	0.019 ± 0.001	2.39748	0.007 ± 0.001	8374 ± 78	3.766 ± 0.125	1.588 ± 0.048	2.96 ± 0.07	180 ± 1	< 120	1.41 ± 0.11	-	0.685 (*)
4567097	1.04853	0.006 ± 0.001	2.09765	0.004 ± 0.001	9849 ± 359	4.205 ± 0.195	2.313 ± 0.046	4.93 ± 0.36	262 ± 2	-	1.32 ± 0.10	2.861 ± 0.102	4.72 ± 0.161
4572373	1.47522	0.021 ± 0.001	2.95112	0.005 ± 0.001	9100 ± 350	3.681 ± 0.290	1.541 ± 0.046	2.38 ± 0.19	177 ± 2	-	1.19 ± 0.10	0.674 ± 0.116	2.28 ± 0.128
4661914	0.97690	0.019 ± 0.001	1.95360	0.008 ± 0.001	7652 ± 281	3.499 ± 0.290	0.975 ± 0.042	1.75 ± 0.13	87 ± 1	-	0.83 ± 0.10	0.981 ± 0.102	0.665 ± 0.1089
4669058	0.10905	0.019 ± 0.012	2.18203	0.003 ± 0.001	8080 ± 281	3.859 ± 0.210	1.054 ± 0.046	1.72 ± 0.12	95 ± 1	-	0.82 ± 0.15	-	0.609 (*)
4818496	1.62697	0.014 ± 0.002	3.25483	0.003 ± 0.001	8857 ± 322	3.687 ± 0.330	1.529 ± 0.042	2.48 ± 0.18	204 ± 3	-	1.01 ± 0.13	0.593 ± 0.264	0.774 ± 0.109
4856799	1.50678	0.022 ± 0.001	3.01300	0.002 ± 0.001	9520 ± 592	3.909 ± 0.225	1.686 ± 0.047	2.56 ± 0.32	196 ± 4	< 120	1.31 ± 0.14	0.531 ± 0.123	0.643 ± 0.107
4857593	1.80324	0.020 ± 0.001	3.60407	0.004 ± 0.001	8279 ± 78	4.116 ± 0.126	1.523 ± 0.053	2.81 ± 0.07	257 ± 4	175 ± 89	1.37 ± 0.11	0.450 ± 0.116	0.618 ± 0.106
4863277	2.07037	0.006 ± 0.002	4.14581	0.002 ± 0.001	9858 ± 355	4.205 ± 0.200	1.682 ± 0.056	2.38 ± 0.18	250 ± 4	207 ± 78	0.64 ± 0.13	-	4.197 (*)
4935271	0.54163	0.034 ± 0.002	1.08881	0.006 ± 0.002	7859 ± 283	4.080 ± 0.145	1.408 ± 0.055	2.73 ± 0.20	75 ± 1	-	1.74 ± 0.13	-	0.799 (*)
4944828	1.09952	0.020 ± 0.001	2.19890	0.007 ± 0.001	7983 ± 80	3.730 ± 0.157	1.382 ± 0.044	2.57 ± 0.07	143 ± 1	< 120	1.26 ± 0.11	0.920 ± 0.104	3.629 ± 0.136
4953140	2.74956	0.022 ± 0.002	5.49926	0.007 ± 0.002	8855 ± 340	3.826 ± 0.250	1.408 ± 0.051	2.15 ± 0.17	300 ± 6	320 ± 39	1.10 ± 0.13	-	8.647 (*)
5039203	1.42323	0.017 ± 0.001	2.84605	0.004 ± 0.001	8204 ± 293	4.020 ± 0.160	1.298 ± 0.047	2.21 ± 0.16	159 ± 2	-	1.00 ± 0.12	-	0.604 (*)
5106287	1.89345	0.015 ± 0.002	3.78851	0.003 ± 0.002	7804 ± 286	3.750 ± 0.228	1.433 ± 0.048	2.85 ± 0.21	273 ± 4	-	1.21 ± 0.13	-	0.619 (*)
5129737	1.17568	0.013 ± 0.001	2.35980	0.004 ± 0.001	8368 ± 298	3.748 ± 0.285	1.809 ± 0.062	3.83 ± 0.28	228 ± 2	-	1.51 ± 0.13	-	0.954 (*)
5213792	2.08696	0.009 ± 0.001	4.21858	0.002 ± 0.001	9769 ± 342	4.213 ± 0.195	1.791 ± 0.053	2.75 ± 0.20	290 ± 4	-	0.90 ± 0.12	-	0.014 (*)
5273195	1.58529	0.005 ± 0.001	3.17646	0.001 ± 0.001	8732 ± 80	3.806 ± 0.165	1.311 ± 0.052	1.98 ± 0.05	159 ± 1	< 120	0.48 ± 0.11	-	0.268 (*)
5288746	1.45866	0.005 ± 0.001	2.91718	0.002 ± 0.001	9153 ± 358	4.106 ± 0.160	1.248 ± 0.045	1.68 ± 0.13	124 ± 2	-	0.41 ± 0.11	-	0.639 (*)
5387719	1.53768	0.020 ± 0.001	3.07791	0.003 ± 0.001	9103 ± 340	3.857 ± 0.240	1.799 ± 0.045	3.20 ± 0.24	249 ± 3	< 120	1.56 ± 0.13	0.633 ± 0.131	0.862 ± 0.110
5392475	0.55034	0.011 ± 0.001	1.15307	0.004 ± 0.001	9211 ± 357	4.077 ± 0.180	1.862 ± 0.057	3.35 ± 0.27	94 ± 1	-	1.21 ± 0.13	-	0.864 (*)
5395418	1.67162	0.033 ± 0.001	3.34623	0.005 ± 0.001	9164 ± 333	3.865 ± 0.245	1.967 ± 0.044	3.82 ± 0.28	323 ± 4	-	2.40 ± 0.13	0.593 ± 0.106	5.188 ± 0.154
5456027	1.24204	0.015 ± 0.001	2.47967	0.008 ± 0.001	8346 ± 280	3.786 ± 0.257	1.417 ± 0.046	2.45 ± 0.17	154 ± 2	-	1.04 ± 0.12	0.817 ± 0.103	4.078 ± 0.171
5524045	1.81517	0.023 ± 0.001	3.63340	0.004 ± 0.001	9500 ± 82	3.869 ± 0.155	1.604 ± 0.043	2.34 ± 0.05	215 ± 2	201 ± 58	1.23 ± 0.10	0.552 ± 0.309	2.328 ± 0.125
5545321	0.86908	0.015 ± 0.003	1.73809	0.008 ± 0.001	7807 ± 596	3.635 ± 0.290	1.043 ± 0.043	1.82 ± 0.28	80 ± 2	< 120	0.77 ± 0.15	1.042 ± 0.116	0.803 ± 0.109
5566579	1.53465	0.025 ± 0.009	3.07023	0.003 ± 0.001	9189 ± 344	4.198 ± 0.150	1.416 ± 0.046	2.02 ± 0.15	157 ± 2	-	1.10 ± 0.15	-	0.522 (*)
5641490	0.97187	0.026 ± 0.001	1.94347	0.004 ± 0.001	9430 ± 83	3.826 ± 0.145	1.644 ± 0.048	2.49 ± 0.06	123 ± 1	< 120	1.39 ± 0.11	-	0.106 (*)
5650229	2.16673	0.022 ± 0.003	4.33197	0.004 ± 0.001	8763 ± 344	3.870 ± 0.240	1.648 ± 0.044	2.90 ± 0.23	318 ± 5	213 ± 61	1.49 ± 0.14	0.429 ± 0.101	0.704 ± 0.111
5730714	0.50930	0.022 ± 0.001	1.01883	0.008 ± 0.001	9765 ± 376	3.646 ± 0.300	2.215 ± 0.057	4.48 ± 0.35	115 ± 1	-	2.29 ± 0.14	1.900 ± 0.124	0.725 ± 0.112
5897685	1.63668	0.016 ± 0.001	3.27303	0.002 ± 0.001	9081 ± 358	4.130 ± 0.158	1.373 ± 0.046	1.97 ± 0.16	163 ± 3	-	0.86 ± 0.12	-	0.633 (*)
5903499	2.48245	0.007 ± 0.001	4.95973	0.002 ± 0.001	9282 ± 357	4.183 ± 0.165	1.363 ± 0.053	1.86 ± 0.15	234 ± 4	-	0.54 ± 0.12	0.347 ± 0.175	0.701 ± 0.107

Table A1 – continued

KIC	f_{rot}	A_{rot}	f_{har}	A_{har}	T_{eff}	$\log g$	$\log(L/L_{\odot})$	R	V_{rot}	$v \sin i$	R_{spot}	P_{ACF}	O: T_{true}	τ_{DT}	
	(d ⁻¹)	(mmag)	(d ⁻¹)	(mmag)	(K)	(dex)	(dex)	(R _⊕)	(km s ⁻¹)	(km s ⁻¹)	(R _E)	(d)		(d)	
5905878	1.25277	0.009 ± 0.001	2.50541	0.003 ± 0.001	8481 ± 302	4.050 ± 0.156	1.161 ± 0.043	1.77 ± 0.13	112 ± 2	-	0.58 ± 0.11	-	0.213 (*)		
5978118	2.57045	0.041 ± 0.001	5.14291	0.006 ± 0.001	9345 ± 351	3.955 ± 0.209	1.602 ± 0.051	2.42 ± 0.19	314 ± 5	312 ± 37	1.69 ± 0.12	0.368 ± 0.186	0.643 ± 0.106		
5980337	1.29218	0.008 ± 0.001	2.58307	0.003 ± 0.001	7825 ± 79	3.984 ± 0.114	-0.044 ± 0.114	0.52 ± 0.68	34 ± 5	< 120	0.16 ± 0.07	-	0.560 (*)		
6062984	1.81630	0.002 ± 0.001	3.64138	0.001 ± 0.001	9348 ± 376	4.009 ± 0.200	1.572 ± 0.045	2.33 ± 0.19	215 ± 3	184 ± 53	0.36 ± 0.10	0.450 ± 0.112	0.663 ± 0.107		
6114539	1.06152	0.012 ± 0.001	2.12341	0.003 ± 0.001	7785 ± 283	4.049 ± 0.150	1.058 ± 0.043	1.86 ± 0.14	100 ± 2	-	0.70 ± 0.12	-	1.783 (*)		
6131612	1.16971	0.006 ± 0.001	2.33885	0.001 ± 0.001	9037 ± 84	3.755 ± 0.185	1.651 ± 0.053	2.73 ± 0.07	162 ± 1	< 120	0.73 ± 0.11	-	3.100 (*)		
6147122	0.95630	0.007 ± 0.001	1.91426	0.007 ± 0.001	7769 ± 270	4.080 ± 0.145	0.980 ± 0.044	1.71 ± 0.12	83 ± 1	-	0.49 ± 0.11	-	1.073 (*)		
6192566	0.75287	0.029 ± 0.008	1.50679	0.009 ± 0.001	7689 ± 270	3.861 ± 0.210	1.655 ± 0.043	3.80 ± 0.27	145 ± 2	< 120	2.23 ± 0.18	1.246 ± 0.103	0.760 ± 0.114		
6222381	1.22897	0.024 ± 0.001	2.45817	0.007 ± 0.001	8597 ± 78	3.761 ± 0.152	1.526 ± 0.045	2.62 ± 0.06	163 ± 1	< 120	1.40 ± 0.11	0.817 ± 0.104	3.623 ± 0.137		
6266219	0.89751	0.017 ± 0.001	1.79499	0.003 ± 0.001	7928 ± 281	4.048 ± 0.156	1.177 ± 0.043	2.06 ± 0.15	94 ± 1	-	0.93 ± 0.10	1.083 ± 0.117	0.892 ± 0.111		
6450107	1.53317	0.008 ± 0.001	3.06111	0.001 ± 0.001	9800 ± 362	4.053 ± 0.190	1.878 ± 0.042	3.02 ± 0.23	234 ± 3	-	0.93 ± 0.10	0.633 ± 0.124	0.865 ± 0.110		
6468647	1.74231	0.016 ± 0.001	3.48446	0.003 ± 0.001	9073 ± 358	4.041 ± 0.169	1.328 ± 0.047	1.87 ± 0.15	165 ± 3	-	0.82 ± 0.12	-	0.557 (*)		
6530137	1.48994	0.015 ± 0.001	2.98002	0.012 ± 0.001	8650 ± 301	4.140 ± 0.140	1.368 ± 0.048	2.15 ± 0.15	163 ± 2	-	0.91 ± 0.12	0.593 ± 0.103	0.662 ± 0.107		
6794857	0.94616	0.021 ± 0.001	1.89270	0.011 ± 0.001	8344 ± 298	3.930 ± 0.205	1.523 ± 0.055	2.77 ± 0.20	132 ± 2	< 120	1.39 ± 0.12	-	0.588 (*)		
6871866	1.04369	0.018 ± 0.001	2.10348	0.013 ± 0.001	7781 ± 270	3.966 ± 0.180	1.098 ± 0.045	1.95 ± 0.14	103 ± 2	-	0.90 ± 0.12	-	0.130 (*)		
6974705	1.61395	0.033 ± 0.001	3.22916	0.007 ± 0.001	8769 ± 334	3.856 ± 0.245	1.568 ± 0.046	2.64 ± 0.20	215 ± 3	-	1.66 ± 0.12	0.613 ± 0.214	0.912 ± 0.110		
7129454	1.93681	0.019 ± 0.001	3.87528	0.003 ± 0.001	9261 ± 357	4.140 ± 0.160	1.606 ± 0.052	2.47 ± 0.20	242 ± 4	249 ± 71	1.18 ± 0.12	0.511 ± 0.115	0.813 ± 0.109		
7375997	1.21081	0.043 ± 0.001	2.42148	0.008 ± 0.001	8554 ± 305	3.780 ± 0.257	1.395 ± 0.048	2.27 ± 0.17	139 ± 2	< 120	1.63 ± 0.10	0.817 ± 0.105	1.739 ± 0.123		
7530366	1.33506	0.021 ± 0.001	2.66863	0.003 ± 0.001	9700 ± 388	3.567 ± 0.325	1.922 ± 0.043	3.24 ± 0.26	218 ± 3	-	1.62 ± 0.10	0.756 ± 0.104	3.380 ± 0.140		
7622596	1.67546	0.008 ± 0.001	3.35245	0.001 ± 0.001	10007 ± 335	3.572 ± 0.265	2.002 ± 0.052	3.34 ± 0.23	283 ± 3	156 ± 57	1.03 ± 0.12	-	7.446 (*)		
7667560	1.54370	0.011 ± 0.001	3.08692	0.003 ± 0.001	8590 ± 323	4.080 ± 0.150	1.188 ± 0.042	1.78 ± 0.14	139 ± 2	-	0.64 ± 0.10	0.633 ± 0.119	0.736 ± 0.109		
7939835	0.63143	0.007 ± 0.001	1.26283	0.002 ± 0.001	7786 ± 286	3.819 ± 0.220	1.278 ± 0.044	2.40 ± 0.18	77 ± 1	< 120	0.69 ± 0.12	-	4.110 (*)		
7959579	1.20814	0.009 ± 0.001	2.41713	0.008 ± 0.001	7696 ± 268	4.043 ± 0.160	1.010 ± 0.042	1.80 ± 0.13	110 ± 2	< 120	0.59 ± 0.10	0.797 ± 0.103	0.696 ± 0.107		
8043385	1.85082	0.017 ± 0.001	3.70975	0.003 ± 0.001	9818 ± 359	4.160 ± 0.200	2.475 ± 0.065	5.99 ± 0.45	547 ± 6	250 ± 73	2.70 ± 0.15	0.511 ± 0.107	0.637 ± 0.106		
8121280	1.34050	0.028 ± 0.001	2.68096	0.008 ± 0.001	8256 ± 274	3.764 ± 0.268	1.291 ± 0.048	2.16 ± 0.15	147 ± 2	-	1.25 ± 0.12	-	1.734 (*)		
8191793	1.64003	0.023 ± 0.002	3.28023	0.008 ± 0.001	8066 ± 283	4.002 ± 0.165	1.526 ± 0.061	2.97 ± 0.22	259 ± 3	139 ± 102	1.56 ± 0.13	-	2.949 (*)		
8330169	1.23067	0.027 ± 0.007	2.46198	0.006 ± 0.002	8075 ± 283	3.741 ± 0.262	1.642 ± 0.048	3.39 ± 0.24	211 ± 2	159 ± 89	1.92 ± 0.17	0.776 ± 0.108	0.682 ± 0.107		
8330740	1.14406	0.032 ± 0.001	2.48480	0.006 ± 0.001	7951 ± 276	4.048 ± 0.156	1.346 ± 0.045	2.49 ± 0.18	144 ± 2	-	1.54 ± 0.12	-	1.519 (*)		
8385850	1.30554	0.011 ± 0.001	2.68508	0.001 ± 0.001	8291 ± 290	3.758 ± 0.289	1.488 ± 0.053	2.69 ± 0.19	178 ± 2	-	0.97 ± 0.12	-	0.603 (*)		
8391713	1.70470	0.009 ± 0.001	3.42719	0.001 ± 0.001	8918 ± 354	3.813 ± 0.278	1.811 ± 0.051	3.38 ± 0.27	291 ± 4	134 ± 100	1.11 ± 0.13	-	0.577 (*)		
8396240	0.98459	0.020 ± 0.002	1.96914	0.005 ± 0.001	7793 ± 278	4.028 ± 0.165	1.208 ± 0.045	2.21 ± 0.16	110 ± 2	-	1.08 ± 0.13	-	$(*)$		
8396309	1.09041	0.023 ± 0.002	2.18707	0.004 ± 0.002	8101 ± 297	3.725 ± 0.294	1.687 ± 0.053	3.55 ± 0.27	196 ± 2	154 ± 104	1.86 ± 0.14	-	1.954 (*)		
8396872	1.43485	0.027 ± 0.001	2.86954	0.004 ± 0.002	8002 ± 280	3.713 ± 0.270	1.918 ± 0.051	4.74 ± 0.34	344 ± 4	< 120	2.69 ± 0.14	0.674 ± 0.133	0.751 ± 0.108		
8453527	1.22669	0.036 ± 0.001	2.45335	0.008 ± 0.001	8141 ± 285	3.725 ± 0.294	1.538 ± 0.044	2.96 ± 0.21	184 ± 2	< 120	1.94 ± 0.12	0.776 ± 0.104	0.764 ± 0.109		
8524728	2.45960	0.022 ± 0.001	4.92597	0.006 ± 0.001	8930 ± 356	3.822 ± 0.265	1.633 ± 0.049	2.74 ± 0.22	342 ± 6	-	1.40 ± 0.12	0.347 ± 0.102	0.678 ± 0.106		
8564695	1.17960	0.010 ± 0.001	2.35883	0.005 ± 0.001	7984 ± 281	3.996 ± 0.178	1.185 ± 0.049	2.05 ± 0.15	122 ± 2	< 120	0.71 ± 0.12	-	4.484 (*)		
8570955	1.64329	0.005 ± 0.001	3.28764	0.002 ± 0.001	8126 ± 283	4.155 ± 0.135	1.102 ± 0.048	1.80 ± 0.13	149 ± 2	-	0.44 ± 0.11	-	1.725 (*)		
8581557	2.07836	0.017 ± 0.001	4.15866	0.003 ± 0.001	8255 ± 297	4.084 ± 0.145	1.323 ± 0.047	2.25 ± 0.17	236 ± 4	197 ± 60	1.01 ± 0.12	0.450 ± 0.397	0.654 ± 0.106		
8586760	1.05307	0.035 ± 0.001	2.10546	0.006 ± 0.001	7785 ± 285	3.702 ± 0.270	1.802 ± 0.047	4.38 ± 0.33	233 ± 2	< 120	2.83 ± 0.14	0.940 ± 0.102	0.928 ± 0.111		
8884276	2.29528	0.029 ± 0.001	4.59533	0.011 ± 0.001	9377 ± 357	3.926 ± 0.230	1.637 ± 0.057	2.50 ± 0.20	290 ± 5	-	1.47 ± 0.12	0.409 ± 0.170	0.644 ± 0.107	</td	

Table A1 – continued

KIC	f_{rot}	A_{rot}	f_{har}	A_{har}	T_{eff}	$\log g$	$\log(L/L_{\odot})$	R	V_{rot}	$v \sin i$	R_{spot}	P_{ACF}	τ_{DT}
	(d ⁻¹)	(mmag)	(d ⁻¹)	(mmag)	(K)	(dex)	(dex)	(R _⊕)	(km s ⁻¹)	(km s ⁻¹)	(R _E)	(d)	(d)
9299980	2.26102	0.028 ± 0.002	4.52171	0.005 ± 0.002	8399 ± 301	3.755 ± 0.280	1.257 ± 0.046	2.01 ± 0.15	230 ± 4	234 ± 73	1.16 ± 0.12	0.409 ± 0.179	0.672 ± 0.107
9304955	1.18183	0.037 ± 0.001	2.36407	0.007 ± 0.001	8086 ± 283	4.008 ± 0.165	1.546 ± 0.050	3.03 ± 0.22	181 ± 2	-	2.01 ± 0.10	-	1.908 (*)
9396171	2.22723	0.051 ± 0.002	4.45429	0.007 ± 0.002	9563 ± 369	4.058 ± 0.205	1.708 ± 0.053	2.61 ± 0.20	294 ± 5	299 ± 47	2.02 ± 0.13	0.450 ± 0.102	3.546 ± 0.141
9418202	0.55205	0.035 ± 0.001	1.11474	0.006 ± 0.001	7763 ± 285	3.683 ± 0.270	1.444 ± 0.050	2.92 ± 0.22	82 ± 1	-	1.89 ± 0.12	-	1.685 (*)
9428798	2.28352	0.016 ± 0.001	4.56549	0.005 ± 0.001	8049 ± 294	4.004 ± 0.157	1.398 ± 0.049	2.58 ± 0.19	298 ± 5	228 ± 65	1.13 ± 0.10	0.347 ± 0.102	0.711 ± 0.107
9453452	1.64741	0.034 ± 0.001	3.29574	0.005 ± 0.001	8664 ± 316	3.901 ± 0.225	1.437 ± 0.044	2.33 ± 0.17	194 ± 3	< 120	1.48 ± 0.12	0.593 ± 0.103	1.016 ± 0.112
9519698	2.44243	0.009 ± 0.001	4.89319	0.001 ± 0.001	9859 ± 345	4.205 ± 0.200	1.806 ± 0.048	2.75 ± 0.20	340 ± 5	< 120	0.90 ± 0.12	0.388 ± 0.115	0.662 ± 0.107
9532445	1.06369	0.019 ± 0.001	2.12729	0.004 ± 0.001	7841 ± 275	3.958 ± 0.178	1.190 ± 0.048	2.14 ± 0.16	115 ± 2	-	1.02 ± 0.12	0.797 ± 0.107	0.667 ± 0.109
9593997	2.16319	0.042 ± 0.001	4.32566	0.053 ± 0.001	7759 ± 275	3.613 ± 0.310	1.105 ± 0.048	1.98 ± 0.15	216 ± 3	147 ± 97	1.40 ± 0.12	0.450 ± 0.119	0.683 ± 0.108
9596469	1.58355	0.040 ± 0.001	3.16867	0.029 ± 0.001	7687 ± 80	3.920 ± 0.120	1.121 ± 0.043	2.05 ± 0.06	164 ± 1	< 120	1.42 ± 0.11	-	0.184 (*)
9655005	0.71508	0.040 ± 0.007	1.42971	0.013 ± 0.001	8086 ± 78	3.732 ± 0.162	1.451 ± 0.049	2.71 ± 0.07	98 ± 1	< 120	1.87 ± 0.12	1.43 ± 0.106	1.505 ± 0.116
9711038	0.67416	0.012 ± 0.001	1.34825	0.003 ± 0.001	7775 ± 294	3.736 ± 0.255	1.154 ± 0.047	2.08 ± 0.16	71 ± 1	< 120	0.79 ± 0.12	-	3.060 (*)
9760777	1.69826	0.031 ± 0.001	3.41022	0.004 ± 0.001	8107 ± 283	3.799 ± 0.224	1.456 ± 0.047	2.71 ± 0.20	233 ± 3	< 120	1.65 ± 0.12	0.572 ± 0.168	0.826 ± 0.109
10068389	1.01706	0.051 ± 0.001	2.03422	0.006 ± 0.002	8647 ± 308	3.787 ± 0.275	1.595 ± 0.043	2.80 ± 0.20	144 ± 2	< 120	2.18 ± 0.12	5.451 ± 0.103	0.554 ± 0.116
10153555	0.94086	0.009 ± 0.001	1.77012	0.005 ± 0.001	7800 ± 270	4.042 ± 0.160	1.253 ± 0.045	2.32 ± 0.17	111 ± 1	-	0.76 ± 0.12	-	0.829 (*)
10156332	1.21457	0.017 ± 0.001	2.42931	0.007 ± 0.001	8501 ± 321	4.211 ± 0.130	1.263 ± 0.049	1.98 ± 0.15	122 ± 3	< 120	0.89 ± 0.12	-	1.342 (*)
10215038	1.40541	0.020 ± 0.001	2.81120	0.006 ± 0.001	9160 ± 78	3.756 ± 0.152	1.486 ± 0.049	2.20 ± 0.05	157 ± 1	< 120	1.07 ± 0.11	-	3.974 (*)
10216016	0.93120	0.029 ± 0.001	1.86244	0.006 ± 0.001	7823 ± 274	4.006 ± 0.170	1.306 ± 0.048	2.45 ± 0.18	116 ± 2	-	1.44 ± 0.12	1.001 ± 0.109	0.879 ± 0.107
10338005	2.09676	0.026 ± 0.001	4.19398	0.006 ± 0.001	10000 ± 357	3.658 ± 0.250	1.989 ± 0.102	3.30 ± 0.25	350 ± 5	-	1.84 ± 0.13	0.409 ± 0.111	0.873 ± 0.104
10354997	1.85626	0.006 ± 0.001	3.71121	0.003 ± 0.001	8698 ± 326	4.001 ± 0.171	1.223 ± 0.043	1.80 ± 0.14	169 ± 3	< 120	0.48 ± 0.12	0.531 ± 0.171	0.835 ± 0.107
10394172	0.75101	0.016 ± 0.003	1.48950	0.005 ± 0.001	9160 ± 346	4.106 ± 0.164	1.479 ± 0.058	2.18 ± 0.17	83 ± 1	-	0.95 ± 0.13	-	1.011 (*)
10405887	1.05742	0.022 ± 0.001	2.11529	0.008 ± 0.001	9282 ± 362	3.877 ± 0.250	1.692 ± 0.053	2.72 ± 0.22	145 ± 2	< 120	1.39 ± 0.12	0.920 ± 0.107	0.820 ± 0.108
10467815	1.42021	0.028 ± 0.001	2.84029	0.004 ± 0.001	8932 ± 358	3.822 ± 0.257	1.354 ± 0.044	1.99 ± 0.16	143 ± 2	< 120	1.15 ± 0.12	0.674 ± 0.109	0.608 ± 0.106
10529091	0.71393	0.037 ± 0.001	1.42817	0.005 ± 0.001	8004 ± 280	3.720 ± 0.275	1.466 ± 0.046	2.82 ± 0.20	102 ± 1	-	1.87 ± 0.12	1.389 ± 0.103	2.853 ± 0.126
10533233	1.13379	0.027 ± 0.002	2.26772	0.005 ± 0.002	9710 ± 374	3.720 ± 0.275	1.797 ± 0.062	2.80 ± 0.22	161 ± 2	< 120	1.59 ± 0.13	0.858 ± 0.105	0.744 ± 0.107
10548172	2.06429	0.014 ± 0.001	4.12846	0.008 ± 0.001	8071 ± 294	4.103 ± 0.133	1.307 ± 0.049	2.31 ± 0.17	241 ± 4	-	0.94 ± 0.12	-	3.537 (*)
10612854	1.52043	0.007 ± 0.001	3.04376	0.002 ± 0.001	8585 ± 82	3.766 ± 0.165	1.460 ± 0.051	2.43 ± 0.06	187 ± 1	< 120	0.70 ± 0.11	-	1.761 (*)
10810140	1.48415	0.009 ± 0.001	2.96864	0.003 ± 0.001	8265 ± 82	3.735 ± 0.210	1.146 ± 0.044	1.83 ± 0.05	137 ± 1	< 120	0.60 ± 0.11	0.654 ± 0.105	0.862 ± 0.108
10816270	1.14221	0.081 ± 0.001	2.29810	0.013 ± 0.001	9345 ± 376	4.027 ± 0.195	1.556 ± 0.048	2.29 ± 0.19	132 ± 2	-	2.25 ± 0.12	0.858 ± 0.104	0.874 ± 0.113
10816278	1.06760	0.009 ± 0.001	2.13659	0.009 ± 0.001	8060 ± 296	3.843 ± 0.215	1.094 ± 0.045	1.81 ± 0.14	98 ± 2	-	0.59 ± 0.12	-	1.306 (*)
10817581	0.99167	0.005 ± 0.001	1.97581	0.003 ± 0.001	8524 ± 306	3.793 ± 0.252	1.462 ± 0.049	2.47 ± 0.18	124 ± 2	-	0.60 ± 0.10	0.920 ± 0.118	0.890 ± 0.108
10879812	1.42972	0.011 ± 0.001	2.85941	0.001 ± 0.001	8250 ± 283	4.089 ± 0.145	1.271 ± 0.042	2.12 ± 0.15	153 ± 3	-	0.77 ± 0.12	0.695 ± 0.193	0.938 ± 0.112
10974769	1.76150	0.029 ± 0.001	3.52144	0.005 ± 0.001	8681 ± 326	3.973 ± 0.185	1.312 ± 0.046	2.00 ± 0.15	179 ± 3	< 120	1.18 ± 0.12	0.572 ± 0.111	0.930 ± 0.111
10990092	0.84952	0.007 ± 0.001	1.70125	0.006 ± 0.001	8059 ± 281	3.731 ± 0.275	1.236 ± 0.047	2.13 ± 0.15	92 ± 1	-	0.62 ± 0.12	-	1.174 (*)
11091033	1.32990	0.013 ± 0.001	2.65951	0.002 ± 0.001	8856 ± 338	4.043 ± 0.170	1.42 ± 0.046	2.18 ± 0.17	147 ± 2	-	0.86 ± 0.11	0.736 ± 0.108	0.898 ± 0.108
11288072	0.88564	0.118 ± 0.001	1.77149	0.018 ± 0.001	8111 ± 285	3.724 ± 0.270	1.514 ± 0.047	2.90 ± 0.21	130 ± 2	124 ± 79	3.44 ± 0.12	1.124 ± 0.103	11.01 ± 0.217
11296464	1.55118	0.015 ± 0.005	3.09483	0.005 ± 0.001	8363 ± 80	3.725 ± 0.160	1.266 ± 0.045	2.05 ± 0.05	161 ± 1	149 ± 51	0.86 ± 0.11	0.633 ± 0.121	0.873 ± 0.101
11303065	0.89503	0.023 ± 0.001	1.79012	0.014 ± 0.001	7679 ± 270	3.818 ± 0.225	0.959 ± 0.043	1.71 ± 0.13	77 ± 1	< 120	0.90 ± 0.11	-	3.985 (*)
11357670	1.35987	0.063 ± 0.001	2.72008	0.026 ± 0.001	8310 ± 79	3.908 ± 0.109	1.213 ± 0.044	1.95 ± 0.05	134 ± 1	< 120	1.69 ± 0.11	0.715 ± 0.102	0.880 ± 0.110
11442175	1.37440	0.013 ± 0.001	2.74830	0.007 ± 0.001	8421 ± 302	3.762 ± 0.280	1.193 ± 0.044	1.86 ± 0.14	129 ± 2	-	0.73 ± 0.12	0.674 ± 0.110	0.644 ± 0.107
11443271	1.27051	0.021 ± 0.001	2.54053	0.009 ± 0.001	8331 ± 277	3.777 ± 0.255	1.784 ± 0.042	3.75 ± 0.25	241 ± 2	180	1.88 ± 0.13	0.797 ± 0.102	9.771 ± 0.176
12072819	1.27417	0.032 ± 0.001	2.54851	0.005 ± 0.001	8145 ± 78	3.954 ± 0.105	1.151 ± 0.045	1.89 ± 0.05	122 ± 1	< 120	1.17 ± 0.11	0.695 ± 0.111	0.880 ± 0.108
12117276	1.50762	0.055 ± 0.001	3.01504	0.056 ± 0.001	7679 ± 76	3.979 ± 0.135	1.358 ± 0.048	2.70 ± 0.07	206 ± 2	129	2.19 ± 0.11	0.654 ± 0.139	0.748 ± 0.108
12155426	0.88528	0.009 ± 0.001	1.71389	0.005 ± 0.001	7882 ± 288	3.712 ± 0.278	1.451 ± 0.047	2.86 ± 0.21	128 ± 2	-	0.94 ± 0.10	-	0.651 (*)
12306265	1.12762	0.006 ± 0.001	2.25611	0.001 ± 0.001	8074 ± 294	3.780 ± 0.250	1.331 ± 0.042	2.37 ± 0.18	135 ± 2	-	0.63 ± 0.10	-	6.083 (*)
12602335	1.47120	0.008 ± 0.001	2.94340	0.007 ± 0.001	8151 ± 306	3.905 ± 0.190	1.382 ± 0.044	2.47 ± 0.19	184 ± 2	< 120	0.76 ± 0.12	0.613 ± 0.110	0.783 ± 0.109

Table A2. List of Am/Fm stars with “hump and spike” features in the frequency spectra. We list the rotation frequency (f_{rot}), rotational velocity (V_{rot}), rotation frequency amplitude (A_{rot}), frequency of the first harmonic of the rotation frequency (f_{har}) and its amplitude (A_{har}) as derived from their frequency spectra, the effective temperature (T_{eff}) and surface gravity ($\log g$) as reported by Mathur et al. (2017), the luminosity ($\log(L/L_{\odot})$) as derived from Gaia parallaxes (Gaia Collaboration 2018), the stellar radius (R) as estimated from the effective temperature and luminosity, the projected rotational velocity ($v \sin i$) as found in the literature (Frasca et al. 2016) in general; Niemczura et al. (2015) for KIC 9117875 and Niemczura et al. (2017) for KIC 9349245, the spot radius (R_{spot}) as estimated from the photometric amplitude, the rotation period (P_{ACF}) and decay-time scale of the starspots (τ_{DT}) as estimated from the autocorrelation functions of their light-curves. (*) marks doubtful measurements.

KIC	f_{rot}	A_{rot}	f_{har}	A_{har}	T_{eff}	$\log g$	$\log(L/L_{\odot})$	R	V_{rot}	$v \sin i$	R_{spot}	P_{ACF}	τ_{DT}
	(d $^{-1}$)	(mmag)	(d $^{-1}$)	(mmag)	(K)	(dex)	(dex)	(R $_{\odot}$)	(km s $^{-1}$)	(km s $^{-1}$)	(R $_{\text{E}}$)	(d)	(d)
3238787	1.72468	0.019 ± 0.004	-	-	6760 ± 81	3.934 ± 0.158	1.305 ± 0.048	3.28 ± 0.10	286 ± 2	< 120	1.56 ± 0.12	-	1.852 (*)
3240406	1.06809	0.005 ± 0.001	2.14095	0.004 ± 0.001	7936 ± 80	4.029 ± 0.110	1.128 ± 0.043	1.94 ± 0.05	105 ± 1	< 120	0.47 ± 0.11	-	1.872 (*)
3956495	1.07119	0.031 ± 0.001	2.13973	0.019 ± 0.001	7021 ± 237	3.827 ± 0.18	1.337 ± 0.131	3.15 ± 0.26	171 ± 2	< 120	1.92 ± 0.13	0.899 ± 0.114	0.711 ± 0.117
4770092	0.73973	0.023 ± 0.002	1.47906	0.016 ± 0.002	6777 ± 205	3.669 ± 0.180	1.183 ± 0.044	2.84 ± 0.18	107 ± 1	< 120	1.49 ± 0.13	-	2.241 (*)
4839729	1.34295	0.009 ± 0.001	2.68266	0.004 ± 0.001	6815 ± 76	4.093 ± 0.125	0.663 ± 0.042	1.54 ± 0.06	105 ± 1	< 120	0.50 ± 0.11	0.797 ± 0.111	1.358 ± 0.128
5121064	0.74769	0.017 ± 0.002	1.49106	0.009 ± 0.002	6666 ± 79	4.114 ± 0.124	1.113 ± 0.046	2.70 ± 0.09	102 ± 1	< 120	1.22 ± 0.11	1.451 ± 0.116	11.674 ± 0.197
6039039	0.89373	0.016 ± 0.001	-	-	7786 ± 79	3.956 ± 0.110	1.250 ± 0.042	2.32 ± 0.06	105 ± 1	< 120	1.01 ± 0.11	-	11.807 (*)
6209721	0.65867	0.010 ± 0.001	1.32945	0.005 ± 0.001	6775 ± 79	4.055 ± 0.138	1.190 ± 0.046	2.86 ± 0.09	95 ± 1	< 120	0.99 ± 0.11	1.349 ± 0.121	0.594 ± 0.118
6804592	0.73354	0.005 ± 0.001	1.46787	0.002 ± 0.001	8557 ± 316	4.094 ± 0.146	1.391 ± 0.045	2.26 ± 0.17	84 ± 1	< 120	0.55 ± 0.12	-	0.902 (*)
6960377	1.03100	0.022 ± 0.001	2.06143	0.006 ± 0.001	7780 ± 286	3.785 ± 0.230	1.239 ± 0.046	2.30 ± 0.17	120 ± 2	< 120	1.18 ± 0.12	-	2.757 (*)
7287683	0.94411	0.008 ± 0.001	1.88856	0.006 ± 0.001	7651 ± 268	4.075 ± 0.150	1.120 ± 0.046	2.07 ± 0.15	99 ± 1	< 120	0.64 ± 0.12	1.042 ± 0.113	0.821 ± 0.119
7287786	0.75129	0.015 ± 0.001	1.50261	0.008 ± 0.001	7864 ± 84	3.841 ± 0.147	0.984 ± 0.048	1.68 ± 0.05	64 ± 1	< 120	0.71 ± 0.11	-	3.685 (*)
7466060	1.09884	0.065 ± 0.005	-	-	6844 ± 242	4.240 ± 0.121	1.253 ± 0.051	3.01 ± 0.22	168 ± 2	< 120	2.65 ± 0.15	1.124 ± 0.177	5.485 ± 0.159
8429756	0.36458	0.031 ± 0.003	0.71879	0.012 ± 0.003	7505 ± 78	4.342 ± 0.067	1.013 ± 0.043	1.90 ± 0.06	35 ± 1	-	1.16 ± 0.11	2.899 ± 0.117	8.402 ± 0.159
8519992	0.45862	0.024 ± 0.003	0.92039	0.012 ± 0.003	6788 ± 271	3.789 ± 0.280	1.313 ± 0.047	3.28 ± 0.27	76 ± 1	< 120	1.75 ± 0.19	2.656 ± 0.116	10.147 ± 0.224
9273647	0.92991	0.011 ± 0.001	1.86037	0.006 ± 0.001	7046 ± 252	3.905 ± 0.250	1.375 ± 0.042	3.27 ± 0.24	154 ± 2	< 120	1.18 ± 0.10	1.103 ± 0.115	4.251 ± 0.152
9906894	1.68073	0.036 ± 0.002	3.36628	0.044 ± 0.002	7615 ± 79	4.045 ± 0.120	1.409 ± 0.047	2.91 ± 0.08	248 ± 2	< 120	1.91 ± 0.11	0.552 ± 0.117	0.782 ± 0.119
10015534	1.19377	0.017 ± 0.002	2.39360	0.005 ± 0.002	8028 ± 294	4.041 ± 0.158	1.057 ± 0.044	1.75 ± 0.13	106 ± 2	< 120	0.79 ± 0.12	1.022 ± 0.115	5.242 ± 0.186
10129532	0.75688	0.006 ± 0.001	1.51573	0.002 ± 0.001	7929 ± 279	3.831 ± 0.225	1.319 ± 0.055	2.42 ± 0.18	93 ± 1	< 120	0.65 ± 0.12	-	1.848 (*)
11027806	1.11659	0.009 ± 0.003	2.22648	0.003 ± 0.003	9080 ± 340	3.405 ± 0.457	2.318 ± 0.087	5.83 ± 0.45	330 ± 3	273 ± 88	1.91 ± 0.19	-	1.196 (*)
11072219	0.87721	0.026 ± 0.002	1.64625	0.008 ± 0.002	6797 ± 193	3.807 ± 0.190	0.675 ± 0.042	1.57 ± 0.10	70 ± 1	< 120	0.87 ± 0.12	1.369 ± 0.116	1.133 ± 0.122
9349245	1.10719	0.005 ± 0.001	2.21412	0.004 ± 0.001	7834 ± 278	3.723 ± 0.294	1.012 ± 0.041	1.74 ± 0.13	98 ± 2	82 ± 2	0.42 ± 0.10	0.879 ± 0.121	0.683 ± 0.118
3459226	0.92658	0.041 ± 0.003	1.85341	0.009 ± 0.003	7280 ± 82	3.622 ± 0.165	0.886 ± 0.046	1.75 ± 0.06	82 ± 1	< 120	1.22 ± 0.11	1.042 ± 0.116	0.860 ± 0.121
9272082	1.03583	0.001 ± 0.001	2.08237	0.001 ± 0.001	9077 ± 333	4.147 ± 0.154	1.852 ± 0.043	3.42 ± 0.25	179 ± 2	< 120	0.37 ± 0.10	-	1.693 (*)
5302167	2.27153	0.007 ± 0.001	4.56527	0.004 ± 0.001	8402 ± 303	3.930 ± 0.190	1.491 ± 0.083	2.63 ± 0.71	302 ± 14	< 120	0.76 ± 0.18	-	1.698 (*)
6116612	0.59486	0.024 ± 0.001	1.18968	0.011 ± 0.001	7012 ± 264	4.088 ± 0.205	0.797 ± 0.043	1.70 ± 0.44	51 ± 2	< 120	0.91 ± 0.15	-	2.100 (*)
8110941	0.78137	0.046 ± 0.010	1.55609	0.010 ± 0.010	7163 ± 257	4.143 ± 0.165	0.840 ± 0.047	1.71 ± 0.46	67 ± 2	< 120	1.27 ± 0.26	1.450 ± 0.188	5.467 ± 0.154
8715392	0.79754	0.016 ± 0.001	1.59484	0.003 ± 0.001	6889 ± 239	3.937 ± 0.295	0.831 ± 0.056	1.83 ± 0.60	74 ± 2	< 120	0.80 ± 0.17	-	4.010 (*)
9426071	0.38520	0.032 ± 0.004	0.76571	0.015 ± 0.004	6706 ± 213	4.226 ± 0.157	0.564 ± 0.029	1.42 ± 0.35	28 ± 1	< 120	0.88 ± 0.18	-	0.808 (*)
11551962	1.70180	0.011 ± 0.002	3.40584	0.004 ± 0.002	6728 ± 225	4.161 ± 0.180	0.065 ± 0.037	1.56 ± 0.43	134 ± 6	< 120	0.59 ± 0.17	0.531 ± 0.128	0.772 ± 0.118
9238276	0.37650	0.270 ± 0.022	0.75927	0.099 ± 0.022	6038 ± 172	4.524 ± 0.126	-0.015 ± 0.060	0.90 ± 0.17	17 ± 1	< 122	1.61 ± 0.19	2.983 ± 0.110	7.202 ± 0.166
4364400	0.36372	0.028 ± 0.003	0.72262	0.010 ± 0.003	5802 ± 165	4.327 ± 0.165	0.129 ± 0.062	1.15 ± 0.27	21 ± 2	-	0.66 ± 0.13	-	1.616 (*)
5726737	0.48377	0.027 ± 0.002	0.95797	0.011 ± 0.002	6015 ± 211	4.196 ± 0.200	0.344 ± 0.020	1.37 ± 0.38	34 ± 4	-	0.78 ± 0.15	1.921 ± 0.128	0.528 ± 0.121
6042168	0.95803	0.024 ± 0.002	1.93109	0.009 ± 0.002	6796 ± 195	3.430 ± 0.215	0.964 ± 0.046	2.19 ± 0.14	106 ± 1	-	1.17 ± 0.12	0.920 ± 0.112	0.814 ± 0.119
7116117	0.94531	0.008 ± 0.001	1.88832	0.001 ± 0.001	7518 ± 276	4.023 ± 0.160	1.097 ± 0.043	2.09 ± 0.16	100 ± 1	-	0.65 ± 0.10	1.022 ± 0.116	0.694 ± 0.119
8655763	1.45803	0.021 ± 0.002	2.91586	0.003 ± 0.002	8235 ± 310	3.665 ± 0.280	1.488 ± 0.052	2.73 ± 0.21	201 ± 3	-	1.37 ± 0.13	-	2.501 (*)
9655438	2.12307	0.126 ± 0.002	4.24670	0.022 ± 0.002	7118 ± 253	4.074 ± 0.184	1.305 ± 0.051	2.96 ± 0.22	318 ± 5	-	3.63 ± 0.13	0.467 ± 0.116	7.489 ± 0.208
10357965	0.63053	0.051 ± 0.002	1.26102	0.026 ± 0.002	7210 ± 275	4.239 ± 0.152	1.368 ± 0.052	3.10 ± 0.24	99 ± 1	-	2.42 ± 0.14	-	1.540 (*)
9117875	0.71566	0.046 ± 0.001	1.43098	0.021 ± 0.001	7300 ± 226	3.931 ± 0.260	1.010 ± 0.050	1.98 ± 0.64	72 ± 2	61 ± 3	1.47 ± 0.16	1.451 ± 0.134	4.852 ± 0.161

REFERENCES

- Abt H. A., 1961, *ApJS*, **6**, 37
 Abt H. A., 2009, *AJ*, **138**, 28
 Abt H. A., Morrell N. I., 1995, *ApJS*, **99**, 135
 Adelman S. J., 1986, *A&AS*, **64**, 173
 Adelman S. J., 2004, in Zverko J., Ziznovsky J., Adelman S. J., Weiss W. W., eds, IAU Symposium Vol. 224, The A-Star Puzzle. pp 1–11, doi:10.1017/S1743921304004314
 Ashoka B. N., et al., 2000, Bulletin of the Astronomical Society of India, **28**, 251
 Aurière M., et al., 2007, *A&A*, **475**, 1053
 Aurière M., et al., 2010, *A&A*, **523**, A40
 Balona L. A., 2012, *MNRAS*, **423**, 3420
 Balona L. A., 2013, *MNRAS*, **431**, 2240
 Balona L. A., 2014, *MNRAS*, **441**, 3543
 Balona L. A., et al., 2011, *MNRAS*, **414**, 792
 Balona L. A., Catanzaro G., Abedigamba O. P., Ripepi V., Smalley B., 2015, *MNRAS*, **448**, 1378
 Balona L. A., Švanda M., Karlický M., 2016, *MNRAS*, **463**, 1740
 Barnes J. R., James D. J., Collier Cameron A., 2002, *Astronomische Nachrichten*, **323**, 333
 Blazère A., et al., 2014, *Proceedings of the International Astronomical Union*, **10**, 67–72
 Blazère A., Neiner C., Petit P., 2016a, *MNRAS*, **459**, L81
 Blazère A., et al., 2016b, *A&A*, **586**, A97
 Boesgaard A. M., Tripicco M. J., 1986, *ApJ*, **303**, 724
 Borucki W. J., et al., 2010, *Science*, **327**, 977
 Bouvier J., 2013, in Hennebelle P., Charbonnel C., eds, EAS Publications Series Vol. 62, EAS Publications Series. pp 143–168 (arXiv:1307.2891), doi:10.1051/eas/1362005
 Braithwaite J., 2014, in Petit P., Jardine M., Spruit H. C., eds, IAU Symposium Vol. 302, Magnetic Fields throughout Stellar Evolution. pp 255–264 (arXiv:1312.4755), doi:10.1017/S1743921314002221
 Brandenburg A., 2000, in Cheng K. S., Chau H. F., Chan K. L., Leung K. C., eds, Astrophysics and Space Science Library Vol. 254, ASSL. p. 1, doi:10.1007/978-94-010-0878-5_1
 Browning M. K., Brun A. S., Toomre J., 2004, *ApJ*, **601**, 512
 Cantiello M., Braithwaite J., 2019, *ApJ*, **883**, 106
 Chowdhury S., Joshi S., Engelbrecht C. A., De Cat P., Joshi Y. C., Paul K. T., 2018, *Ap&SS*, **363**, 260
 Claverie A., Isaak G. R., McLeod C. P., van der Raay H. B., Roca Cortes T., 1981, *Nature*, **293**, 443
 Collier Cameron A., 1995, *MNRAS*, **275**, 534
 Conti P. S., 1970, *PASP*, **82**, 781
 Costa G., Girardi L., Bressan A., Marigo P., Rodrigues T. S., Chen Y., Lanza A., Goudfrooij P., 2019, *MNRAS*, **485**, 4641
 De Cat P., et al., 2015, *ApJS*, **220**, 19
 Debernardi Y., 2000, in IAU Symposium. p. 161
 Dupret M. A., Grigahcène A., Garrido R., Gabriel M., Scuflaire R., 2004, *A&A*, **414**, L17
 Dziembowski W., Krolikowska M., Kosovichev A., 1988, *Acta Astron.*, **38**, 61
 Fossati L., Bagnulo S., Landstreet J., Wade G., Kochukhov O., Monier R., Weiss W., Gebran M., 2008, *A&A*, **483**, 891
 Fossati L., Ryabchikova T., Bagnulo S., Alecian E., Grunhut J., Kochukhov O., Wade G., 2009, *A&A*, **503**, 945
 Frasca A., Alcalá J. M., Covino E., Catalano S., Marilli E., Paladino R., 2003, *A&A*, **405**, 149
 Frasca A., Guillout P., Marilli E., Freire Ferrero R., Biazzo K., Klutsch A., 2006, *A&A*, **454**, 301
 Frasca A., et al., 2016, *A&A*, **594**, A39
 Gaia Collaboration 2018, VizieR Online Data Catalog, p. I/345
 Gebran M., Farah W., Paletou F., Monier R., Watson V., 2016, *A&A*, **589**, A83
 Giampapa M. S., Rosner R., 1984, *ApJ*, **286**, L19
 Giles H. A. C., Collier Cameron A., Haywood R. D., 2017, *MNRAS*, **472**, 1618
 Gray R. O., et al., 2016, *AJ*, **151**, 13
 Green G. M., 2018, *JOSS*, **3**, 695
 Green G. M., Schlafly E. F., Zucker C., Speagle J. S., Finkbeiner D. P., 2019, arXiv e-prints, p. arXiv:1905.02734
 Howell S. B., et al., 2014, *PASP*, **126**, 398
 Hui-Bon-Hoa A., 2000, *A&AS*, **144**, 203
 Jenkins J. M., et al., 2010, *ApJ*, **713**, L120
 Joshi S., et al., 2003, *MNRAS*, **344**, 431
 Joshi S., Mary D. L., Martinez P., Kurtz D. W., Girish V., Seetha S., Sagar R., Ashoka B. N., 2006, *A&A*, **455**, 303
 Joshi S., Mary D. L., Chakradhari N. K., Tiwari S. K., Billaud C., 2009, *A&A*, **507**, 1763
 Joshi S., Ryabchikova T., Kochukhov O., Sachkov M., Tiwari S. K., Chakradhari N. K., Piskunov N., 2010, *MNRAS*, **401**, 1299
 Joshi S., et al., 2012, *MNRAS*, **424**, 2002
 Joshi S., et al., 2016, *A&A*, **590**, A116
 Joshi S., Semenko E., Moiseeva A., Sharma K., Joshi Y. C., Sachkov M., Singh H. P., Yerra B. K., 2017, *MNRAS*, **467**, 633
 Kaler J. B., 1989, Stars and their spectra. an introduction to spectral sequence
 Khalack V. R., LeBlanc F., 2015, Advances in Astronomy and Space Physics, **5**, 3
 Khokhlova V. L., 1981, in Liege International Astrophysical Colloquia. pp 457–463
 Koch D. G., et al., 2010, *ApJL*, **713**, L79
 Krivova N. A., Solanki S. K., Fligge M., Unruh Y. C., 2003, *A&A*, **399**, L1
 Kron G. E., 1947, *PASP*, **59**, 261
 Kunzli M., North P., 1998, *A&AS*, **127**, 277
 Lenz P., Breger M., 2005, *CoAst*, **146**, 53
 Lignières F., Petit P., Böhm T., Aurière M., 2009, *A&A*, **500**, L41
 Martinez P., et al., 2001, *A&A*, **371**, 1048
 Mathur S., et al., 2017, *ApJS*, **229**, 30
 McQuillan A., Aigrain S., Mazeh T., 2013, *MNRAS*, **432**, 1203
 McQuillan A., Mazeh T., Aigrain S., 2014, *ApJS*, **211**, 24
 Michaud G., 1970, *ApJ*, **160**, 641
 Monier R., 2019, *Research Notes of the AAS*, **3**, 118
 Mossner B., Baudin F., Lanza A. F., Hulot J. C., Catala C., Baglin A., Auvergne M., 2009, *A&A*, **506**, 245
 Mullan D. J., 1973, *Irish Astronomical Journal*, **11**, 32
 Murphy S. J., 2014, PhD thesis, Jeremiah Horrocks Institute, University of Central Lancashire, Preston, UK <EMAIL>murphy@physics.usyd.edu.au</EMAIL>
 Murphy S. J., Hey D., Van Reeth T., Bedding T. R., 2019, *MNRAS*, **485**, 2380
 Neiner C., Lampens P., 2015, *MNRAS*, **454**, L86
 Neiner C., Wade G. A., Sikora J., 2017, *MNRAS*, **468**, L46
 Niemczura E., et al., 2015, *MNRAS*, **450**, 2764
 Niemczura E., et al., 2017, *MNRAS*, **470**, 2870
 North P., Ginestet N., Carquillat J.-M., Carrier F., Udry S., 1998, Contributions of the Astronomical Observatory Skalnate Pleso, **27**, 179
 Noyes R. W., Hartmann L. W., Baliunas S. L., Duncan D. K., Vaughan A. H., 1984, *ApJ*, **279**, 763
 Papaloizou J., Pringle J. E., 1978, *MNRAS*, **182**, 423
 Pedersen M. G., Antoci V., Korhonen H., White T. R., Jessen-Hansen J., Lehtinen J., Nikbaksh S., Viuho J., 2017, *MNRAS*, **466**, 3060
 Petit P., et al., 2010, *A&A*, **523**, A41
 Petit P., et al., 2011, *A&A*, **532**, L13
 Petit P., et al., 2014, *A&A*, **568**, C2
 Petit P., Hébrard E. M., Böhm T., Folsom C. P., Lignières F., 2017, *MNRAS*, **472**, L30
 Power J., Wade G. A., Hanes D. A., Aurier M., Silvester J., 2007, in Romanyuk I. I., Kudryavtsev D. O., Neizvestnaya

- O. M., Shapoval V. M., eds, Physics of Magnetic Stars. p. 89
 ([arXiv:astro-ph/0612557](https://arxiv.org/abs/astro-ph/0612557))
- Preston G. W., 1974, *ARA&A*, **12**, 257
- Renson P., 1988, *A&AS*, **76**, 127
- Ricker G. R., et al., 2014, *JATIS*, **1**, 14003
- Royer F., Zorec J., Gómez A. E., 2007, *A&A*, **463**, 671
- Ryabchikova T., Piskunov N., Kochukhov O., Tsymbal V., Mittermayer P., Weiss W. W., 2002, *A&A*, **384**, 545
- Saio H., 1981, *ApJ*, **244**, 299
- Saio H., Kurtz D. W., Murphy S. J., Antoci V. L., Lee U., 2018, *MNRAS*, **474**, 2774
- Sills A., Deliyannis C. P., 2000, *ApJ*, **544**, 944
- Smalley B., et al., 2014, *A&A*, **564**, A69
- Smith J. C., et al., 2012, *PASP*, **124**, 1000
- Soufi F., Goupil M. J., Dziembowski W. A., 1998, *A&A*, **334**, 911
- Stateva I. K., Iliev I. K., Budaj J., Barzova I. S., 2009, *BAJ*, **12**, 29
- Strassmeier K. G., 2009, *The Astronomy and Astrophysics Review*, **17**, 251
- Stumpe M. C., et al., 2012, *PASP*, **124**, 985
- Stumpe M. C., Smith J. C., Catanzarite J. H., Van Cleve J. E., Jenkins J. M., Twicken J. D., Girouard F. R., 2014, *PASP*, **126**, 100
- Swan P. R., 1982, *AJ*, **87**, 1608
- Takeda Y., Han I., Kang D.-I., Lee B.-C., Kim K.-M., 2008, *Journal of Korean Astronomical Society*, **41**, 83
- Théado S., Vauclair S., Alecian G., LeBlanc F., 2011, in Alecian G., Belkacem K., Samadi R., Valls-Gabaud D., eds, SF2A-2011: Proceedings of the Annual meeting of the French Society of Astronomy and Astrophysics. pp 253–256
- Thompson S. E., Fraquelli D., Van Cleve J. E., Caldwell D. A., 2016, Technical report, Kepler Archive Manual
- Turcotte S., 2001, arXiv e-prints, [pp astro-ph/0111179](https://arxiv.org/abs/astro-ph/0111179)
- Turcotte S., 2003, in Balona L. A., Henrichs H. F., Medupe R., eds, Astronomical Society of the Pacific Conference Series Vol. 305, Magnetic Fields in O, B and A Stars: Origin and Connection to Pulsation, Rotation and Mass Loss. p. 199
 ([arXiv:astro-ph/0304424](https://arxiv.org/abs/astro-ph/0304424))
- Vauclair G., 1976, *A&A*, **50**, 435
- Watson W. D., 1970, *ApJL*, **162**, L45

This paper has been typeset from a TeX/LaTeX file prepared by the author.